

A Deeper Look at Discounting Mismatch in Actor-Critic Algorithms

Shangdong Zhang
University of Oxford
shangdong.zhang@cs.ox.ac.uk

Romain Laroche
Microsoft Research Montreal
romain.laroche@microsoft.com

Harm van Seijen
Microsoft Research Montreal
harm.vanseijen@microsoft.com

Shimon Whiteson
University of Oxford
shimon.whiteson@cs.ox.ac.uk

Remi Tachet des Combes
Microsoft Research Montreal
remi.tachet@microsoft.com

ABSTRACT

We investigate the discounting mismatch in actor-critic algorithm implementations from a representation learning perspective. Theoretically, actor-critic algorithms usually have discounting for both the actor and critic, *i.e.*, there is a γ^t term in the actor update for the transition observed at time t in a trajectory and the critic is a discounted value function. Practitioners, however, usually ignore the discounting (γ^t) for the actor while using a discounted critic. We investigate this mismatch in two scenarios. In the first scenario, we consider optimizing an undiscounted objective ($\gamma = 1$) where γ^t disappears naturally ($1^t = 1$). We then propose to interpret the discounting in the critic in terms of a *bias-variance-representation* trade-off and provide supporting empirical results. In the second scenario, we consider optimizing a discounted objective ($\gamma < 1$) and propose to interpret the omission of the discounting in the actor update from an *auxiliary task* perspective and provide supporting empirical results.

KEYWORDS

Actor Critic; Discount Factor; Reinforcement Learning

ACM Reference Format:

Shangdong Zhang, Romain Laroche, Harm van Seijen, Shimon Whiteson, and Remi Tachet des Combes. 2022. A Deeper Look at Discounting Mismatch in Actor-Critic Algorithms. In *Proc. of the 21st International Conference on Autonomous Agents and Multiagent Systems (AAMAS 2022)*, Online, May 9–13, 2022, IFAAMAS, 27 pages.

1 INTRODUCTION

Actor-critic algorithms have enjoyed great success both theoretically (Konda [22], Schulman et al. [36], Sutton et al. [43], Williams [51]) and empirically (Mnih et al. [30], OpenAI [32], Schulman et al. [38], Silver et al. [39]). There is, however, a longstanding gap between the theory behind actor-critic algorithms and how practitioners implement them. Let γ , γ_A , and γ_C be the discount factors for defining the objective, updating the actor, and updating the critic respectively. Theoretically, no matter whether $\gamma = 1$ or $\gamma < 1$, we should always use $\gamma_A = \gamma_C = \gamma$ (Schulman et al. [36], Sutton et al. [43]) or at least keep $\gamma_A = \gamma_C$ if Blackwell optimality (Veinott

[49], Weitzman [50])¹ is considered. Practitioners, however, usually use $\gamma_A = 1$ and $\gamma_C < 1$ in their implementations (Achiam [1], Caspi et al. [9], Dhariwal et al. [12], Kostrikov [23], Liang et al. [28], Stooke and Abbeel [40], Zhang [55]). Although this mismatch and its theoretical disadvantage have been recognized by Nota and Thomas [31], Thomas [45], whether and why it yields benefits in practice has not been systematically studied. In this paper, we empirically investigate this mismatch from a representation learning perspective. We consider two scenarios separately.

SCENARIO 1. *The true objective is undiscounted ($\gamma = 1$)*

The theory prescribes to use $\gamma_A = \gamma_C = \gamma = 1$. Practitioners, however, usually use $\gamma_A = \gamma = 1$ but $\gamma_C < 1$, introducing *bias*. We explain the benefits from this mismatch with the following hypothesis:

HYPOTHESIS 1. $\gamma_C < 1$ optimizes a *bias-variance-representation* trade-off.

It is easy to see that $\gamma_C < 1$ reduces the variance in bootstrapping targets. We also provide empirical evidence showing that when $\gamma_C < 1$, it may become easier to find a good representation than when $\gamma_C = 1$ for reasons beyond the reduced variance. Consequently, although using $\gamma_C < 1$ introduces bias, it can facilitate representation learning. For our empirical study, we make use of fixed horizon temporal difference learning (De Asis et al. [11]) to disentangle the various effects of the discount factor on the learning process.

SCENARIO 2. *The true objective function is discounted: $\gamma = \gamma_C < 1$.*

Theoretically, there is a γ^t term for the actor update on a transition observed at time t in a trajectory (Schulman et al. [36], Sutton et al. [43]). Practitioners, however, usually ignore this term while using a discounted critic, *i.e.*, $\gamma_A = 1$ and $\gamma_C = \gamma < 1$ are used. We explain this mismatch with the following hypothesis:

HYPOTHESIS 2. *The possible performance improvement of the biased setup (*i.e.*, $\gamma_C = \gamma < 1$ and $\gamma_A = 1$) over the unbiased setup (*i.e.*, $\gamma_C = \gamma_A = \gamma < 1$) comes from improved representation learning.*

Our empirical study involves implementing the difference between the biased and unbiased setup as an auxiliary task such that the difference contributes to the learning process through only representation learning. We also design new benchmarking environments where the sign of the reward function is flipped after a certain time step such that later transitions differ from earlier ones. In that setting, the unbiased setup outperforms the biased setup.

Proc. of the 21st International Conference on Autonomous Agents and Multiagent Systems (AAMAS 2022), P. Faliszewski, V. Mascardi, C. Pelachaud, M.E. Taylor (eds.), May 9–13, 2022, Online. © 2022 International Foundation for Autonomous Agents and Multiagent Systems (www.ifaamas.org). All rights reserved.

¹Blackwell optimality states that, in finite MDPs, there exists a $\gamma_0 < 1$ such that for all $\gamma \geq \gamma_0$, the optimal policies for the γ -discounted objective are the same.

2 BACKGROUND

Markov Decision Processes: We consider an infinite horizon MDP with a finite state space \mathcal{S} , a finite action space \mathcal{A} , a bounded reward function $r : \mathcal{S} \rightarrow \mathbb{R}$, a transition kernel $p : \mathcal{S} \times \mathcal{S} \times \mathcal{A} \rightarrow [0, 1]$, an initial state distribution μ_0 , and a discount factor $\gamma \in [0, 1]$.² The initial state S_0 is sampled from μ_0 . At time step t , an agent in state S_t takes action $A_t \sim \pi(\cdot|S_t)$, where $\pi : \mathcal{A} \times \mathcal{S} \rightarrow [0, 1]$ is the policy it follows. The agent then gets a reward $R_{t+1} \doteq r(S_t)$ and proceeds to the next state $S_{t+1} \sim p(\cdot|S_t, A_t)$. The return of the policy π at time step t is defined as

$$G_t \doteq \sum_{i=1}^{\infty} \gamma^{i-1} R_{t+i},$$

which allows us to define the state value function

$$v_{\pi}^{\gamma}(s) \doteq \mathbb{E}[G_t | S_t = s]$$

and the state-action value function

$$q_{\pi}^{\gamma}(s, a) \doteq \mathbb{E}[G_t | S_t = s, A_t = a].$$

We consider episodic tasks where we assume there is an absorbing state $s^{\infty} \in \mathcal{S}$ such that $r(s^{\infty}) = 0$ and $p(s^{\infty}|s^{\infty}, a) = 1$ holds for any $a \in \mathcal{A}$. When $\gamma < 1$, v_{π}^{γ} and q_{π}^{γ} are always well defined. When $\gamma = 1$, to ensure v_{π}^{γ} and q_{π}^{γ} are well defined, we further assume finite expected episode length. Let T_s^{π} be a random variable denoting the first time step that an agent hits s^{∞} when following π given $S_0 = s$. We assume $T_{\max} \doteq \sup_{\pi \in \Pi} \max_s \mathbb{E}[T_s^{\pi}] < \infty$, where π is parameterized by θ and Π is the corresponding function class. Similar assumptions are also used in stochastic shortest path problems (e.g., Section 2.2 of Bertsekas and Tsitsiklis [7]). In our experiments, all the environments have a hard time limit of 1000, i.e., $T_{\max} = 1000$. This is standard practice; classic RL environments also have an upper limit on their episode lengths (e.g. 27k in Bellemare et al. [5, ALE]). Following Pardo et al. [34], we add the (normalized) time step t in the state to keep the environment Markovian under the presence of the hard time limit. We measure the performance of a policy π with

$$J_Y(\pi) \doteq \mathbb{E}_{S_0 \sim \mu_0}[v_{\pi}^{\gamma}(S_0)].$$

Vanilla Policy Gradient: Sutton et al. [43] compute $\nabla_{\theta} J_Y(\pi)$ as

$$\nabla_{\theta} J_Y(\pi) \doteq \sum_s d_{\pi}^{\gamma}(s) \sum_a q_{\pi}^{\gamma}(s, a) \nabla_{\theta} \pi(a|s), \quad (1)$$

where

$$d_{\pi}^{\gamma}(s) \doteq \begin{cases} \sum_{t=0}^{\infty} \gamma^t \Pr(S_t = s | \mu_0, p, \pi), & \gamma < 1 \\ \mathbb{E}[\sum_{t=0}^{T_{S_0}^{\pi}} \Pr(S_t = s | S_0, p, \pi)], & \gamma = 1 \end{cases}.$$

Note d_{π}^{γ} remains well-defined for $\gamma = 1$ when $T_{\max} < \infty$. In order to optimize the policy performance $J_Y(\pi)$, one can follow (1) and, at time step t , update θ_t as

$$\theta_{t+1} \leftarrow \theta_t + \alpha \gamma_A^t q_{\pi}^{\gamma_c}(S_t, A_t) \nabla_{\theta} \log \pi(A_t | S_t), \quad (2)$$

where α is a learning rate. If we replace $q_{\pi}^{\gamma_c}$ with a learned value function, the update rule (2) becomes an actor-critic algorithm, where the actor refers to π and the critic refers to the learned approximation of $q_{\pi}^{\gamma_c}$. In practice, an estimate for $v_{\pi}^{\gamma_c}$ instead of $q_{\pi}^{\gamma_c}$ is usually learned. Theoretically, we should have $\gamma_A = \gamma_c = \gamma$.

²Following Schulman et al. [36], we consider $r : \mathcal{S} \rightarrow \mathbb{R}$ instead of $r : \mathcal{S} \times \mathcal{A} \rightarrow \mathbb{R}$ for simplicity.

Practitioners, however, usually ignore the γ_A^t term in (2), and use $\gamma_c < \gamma_A = 1$. What this update truly optimizes remains an open problem (Nota and Thomas [31]).

TRPO and PPO: To improve the stability of actor-critic algorithms, Schulman et al. [36] propose Trust Region Policy Optimization (TRPO), based on the performance improvement lemma:

LEMMA 2.1. (Theorem 1 in Schulman et al. [36]) For $\gamma < 1$ and any two policies π and π' ,

$$J_Y(\pi') \geq J_Y(\pi) + \sum_s d_{\pi}^{\gamma}(s) \sum_a \pi'(a|s) \text{Adv}_{\pi}^{\gamma}(s, a) - \frac{4 \max_{s,a} |\text{Adv}_{\pi}^{\gamma}(s, a)| \gamma \epsilon(\pi, \pi')}{(1-\gamma)^2},$$

where

$$\text{Adv}_{\pi}^{\gamma}(s, a) \doteq \mathbb{E}_{s' \sim p(\cdot|s, a)} [r(s) + \gamma v_{\pi}^{\gamma}(s') - v_{\pi}^{\gamma}(s)]$$

is the advantage,

$$\epsilon(\pi, \pi') \doteq \max_s D_{KL}(\pi(\cdot|s) || \pi'(\cdot|s)),$$

and D_{KL} refers to the KL divergence.

To facilitate our empirical study, we first make a theoretical contribution by extending Lemma 2.1 to the undiscounted setting. We have the following lemma:

LEMMA 2.2. Assuming $T_{\max} < \infty$, for $\gamma = 1$ and any two policies π and π' , we have

$$J_Y(\pi') \geq J_Y(\pi) + \sum_s d_{\pi}^{\gamma}(s) \sum_a \pi'(a|s) \text{Adv}_{\pi}^{\gamma}(s, a) - 4 \max_{s,a} |\text{Adv}_{\pi}^{\gamma}(s, a)| T_{\max}^2 \epsilon(\pi, \pi').$$

The proof of Lemma 2.2 is provided in the appendix. A practical implementation of Lemmas 2.1 and 2.2 is to compute a new policy θ via gradient ascent on the clipped objective:

$$L(\theta) \doteq \sum_{t=0}^{\infty} \gamma_A^t L_t(\theta, \theta_{\text{old}}), \quad (3)$$

where

$$L_t(\theta, \theta_{\text{old}}) \doteq \min \left\{ \frac{\pi_{\theta}(A_t|S_t)}{\pi_{\theta_{\text{old}}}(A_t|S_t)} \text{Adv}_{\pi_{\theta_{\text{old}}}}^{\gamma_c}(S_t, A_t), \right. \\ \left. \text{clip}\left(\frac{\pi_{\theta}(A_t|S_t)}{\pi_{\theta_{\text{old}}}(A_t|S_t)}\right) \text{Adv}_{\pi_{\theta_{\text{old}}}}^{\gamma_c}(S_t, A_t) \right\}.$$

Here S_t and A_t are sampled from $\pi_{\theta_{\text{old}}}$, and

$$\text{clip}(x) \doteq \max(\min(x, 1 + \epsilon), 1 - \epsilon)$$

with ϵ a hyperparameter. Theoretically, we should have $\gamma_A = \gamma_c$, but practical algorithms like Proximal Policy Optimization (PPO, Schulman et al. [38]) usually use $\gamma_c < \gamma_A = 1$.

Policy Evaluation: We now introduce several policy evaluation techniques we use in our empirical study. Let \hat{v} be our estimate of v_{π}^{γ} . At time step t , Temporal Difference learning (TD, Sutton [41]) updates \hat{v} as

$$\hat{v}(S_t) \leftarrow \hat{v}(S_t) + \alpha(R_{t+1} + \gamma \hat{v}(S_{t+1}) - \hat{v}(S_t)).$$

Instead of the infinite horizon discounted return G_t , De Asis et al. [11] propose to consider the H -step return

$$G_t^H \doteq \sum_{i=1}^H R_{t+i}.$$

Correspondingly, the H -step value function is defined as

$$v_{\pi}^H(s) \doteq \mathbb{E}[G_t^H | S_t = s].$$

We let \hat{v}^H be our estimate of v_π^H . At time step t , De Asis et al. [11] use the following update rule to learn \hat{v}^H . For $i = 1, \dots, H$:

$$\hat{v}^i(S_t) \leftarrow \hat{v}^i(S_t) + \alpha(R_{t+1} + \hat{v}^{i-1}(S_{t+1}) - \hat{v}^i(S_t)), \quad (4)$$

where $\hat{v}^0(s) \doteq 0$. In other words, to learn \hat{v}^H , we need to learn $\{\hat{v}^i\}_{i=1, \dots, H}$ simultaneously. De Asis et al. [11] call (4) *Fixed Horizon Temporal Difference learning* (FHTD).

Methodology: We consider MuJoCo (Todorov et al. [46]) robot simulation tasks from OpenAI gym (Brockman et al. [8]) as our benchmark. Given its popularity in understanding deep RL algorithms (Andrychowicz et al. [4], Engstrom et al. [13], Henderson et al. [17], Ilyas et al. [18]) and designing new deep RL algorithms (Fujimoto et al. [15], Haarnoja et al. [16]), we believe our empirical results are relevant to most practitioners.

We choose PPO, a simple yet effective and widely used algorithm, as the representative actor-critic algorithm for our empirical study. PPO is usually equipped with generalized advantage estimation (GAE, Schulman et al. [37]), which has a tunable hyperparameter γ . The roles of γ and $\hat{\gamma}$ are similar. To reduce its confounding effect, we do not use GAE in our experiments, *i.e.*, the advantage estimation for our actor is simply the TD error $R_{t+1} + \gamma_C \hat{v}(S_{t+1}) - \hat{v}(S_t)$. The PPO pseudocode we follow is provided in Algorithm 1 in the appendix and we refer to it as the default PPO implementation.

We use the standard architecture and optimizer across all tasks. In particular, the actor and the critic do not share layers. We conduct a thorough grid search for the learning rate of each algorithmic configuration (*i.e.*, for every curve in all figures). All experimental details are provided in the appendix. We report the average episode return of the ten most recent episodes against the number of interactions with the environment. Curves are averages over 30 independent runs with shaded regions indicating standard errors. All our implementations and our Docker environment are publicly available for future research.³

3 OPTIMIZING THE UNDISCOUNTED OBJECTIVE (SCENARIO 1)

In this scenario, the goal is to optimize the *undiscounted* objective $J_{\gamma=1}(\pi)$. This scenario is related to most practitioners as they usually use the undiscounted return as the performance metric (Haarnoja et al. [16], Mnih et al. [30], Schulman et al. [38]). One theoretically grounded option is to use $\gamma_A = \gamma_C = \gamma = 1$. By using $\gamma_A = 1$ and $\gamma_C < 1$, practitioners introduce *bias*. We first empirically confirm that introducing bias in this way indeed has empirical advantages. A simple first hypothesis for this is that $\gamma_C < 1$ leads to lower variance in Monte Carlo return bootstrapping targets than $\gamma_C = 1$; it thus optimizes a bias-variance trade-off. However, we further show that there are empirical advantages from $\gamma_C < 1$ that cannot be explained solely by this bias-variance trade-off, indicating that there are additional factors beyond variance. We then show empirical evidence identifying representation learning as an additional factor, leading to the *bias-variance-representation* trade-off from Hypothesis 1. All the experiments in this section use $\gamma_A = 1$.

Bias-variance trade-off: To investigate the advantages of using $\gamma_C < 1$, we first test default PPO with $\gamma_C \in \{0.95, 0.97, 0.99, 0.995, 1\}$. We find that the best discount factor is always with $\gamma_C < 1$ and that

$\gamma_C = 1$ usually leads to a performance drop (Figure 1). In default PPO, although the advantage is computed as the one-step TD error, the update target for updating the critic $\hat{v}(S_t)$ is almost always a Monte Carlo return, *i.e.*, $\sum_{i=t+1}^{T_{\max}} \gamma_C^{i-t-1} R_i$. Here γ_C has a gating effect in controlling the variance of the Monte Carlo return: when γ_C is smaller, the randomness from R_i contributes less to the variance of the Monte Carlo return. In this paper, we refer to this gating effect as *variance control*. As the objective is undiscounted and we use $\gamma_A = \gamma = 1$, theoretically we should also use $\gamma_C = 1$ when computing the Monte Carlo return if we do not want to introduce bias. By using $\gamma_C < 1$, bias is introduced. The variance of the Monte Carlo return is, however, also reduced. Consequently, a simple hypothesis for the empirical advantage of using $\gamma_C < 1$ is that it optimizes a bias-variance trade-off. We find, however, that there is more at play.

Beyond bias-variance trade-off: To make other possible effects of γ_C pronounced, it is desirable to reduce the variance control effect of γ_C . To this end, we benchmark PPO-TD (Algorithm 2 in the appendix). PPO-TD is the same as default PPO except that the critic is updated with one-step TD, *i.e.*, the update target for $\hat{v}(S_t)$ is now $R_{t+1} + \gamma_C \hat{v}(S_{t+1})$. In this update target, γ_C gates the randomness from only the immediate successor state S_{t+1} . By contrast, in the original Monte Carlo update target, γ_C gates the randomness of all future states and rewards. Figure 2 shows that PPO-TD ($\gamma_C = 1$) outperforms PPO ($\gamma_C = 1$) in four games. This indicates that PPO-TD might be less vulnerable to the large variance in critic update targets introduced by using $\gamma_C = 1$ than default PPO. Figure 3 suggests, however, that even for PPO-TD, $\gamma_C < 1$ is still preferable to $\gamma_C = 1$.

Of course, in PPO-TD, γ_C still has the variance control effect, though not as pronounced as that in default PPO. To make other possible effects of γ_C more pronounced, we benchmark PPO-TD-Ex (Algorithm 3 in the appendix), in which we provide N extra transitions to the critic by sampling multiple actions at any single state and using an averaged bootstrapping target. The update target for $\hat{v}(S_t)$ in PPO-TD-Ex is

$$\frac{1}{N+1} \sum_{i=0}^N R_{t+1}^i + \gamma_C \hat{v}(S_{t+1}^i).$$

Here R_{t+1}^0 and S_{t+1}^0 refer to the original reward and successor state. To get R_{t+1}^i and S_{t+1}^i for $i \in \{1, \dots, N\}$, we first sample an action A_t^i from the sampling policy, then reset the environment to S_t , and finally execute A_t^i to get R_{t+1}^i and S_{t+1}^i . The advantage for the actor update in PPO-TD-Ex is estimated with $R_{t+1}^0 + \hat{v}(S_{t+1}^0) - \hat{v}(S_t)$ regardless of γ_C to further depress its variance control effect. Importantly, we do not count those N extra transitions in the x -axis when plotting. If we use the true value function instead of \hat{v} , $N \geq 1$ should always outperform $N = 0$ as the additional transitions help reduce variance (assuming γ_C is fixed). However, in practice we have only \hat{v} , which is not trained on the extra successor states $\{S_{t+1}^i\}_{i=1, \dots, N}$. So the quality of the prediction $\hat{v}(S_{t+1}^i)$ depends mainly on the generalization of \hat{v} . Consequently, increasing N risks potential erroneous prediction $\hat{v}(S_{t+1}^i)$. That being said, though not guaranteed to improve the performance, when the prediction $\hat{v}(S_{t+1}^i)$ is decent, increasing N should at least not lead to a performance drop. As shown by Figure 4, PPO-TD-Ex ($\gamma_C = 0.99$) roughly follows this intuition. However, surprisingly, providing any extra transition this way to PPO-TD-Ex ($\gamma_C = 1$) leads to a significant performance drop

³<https://github.com/ShangtongZhang/DeepRL>

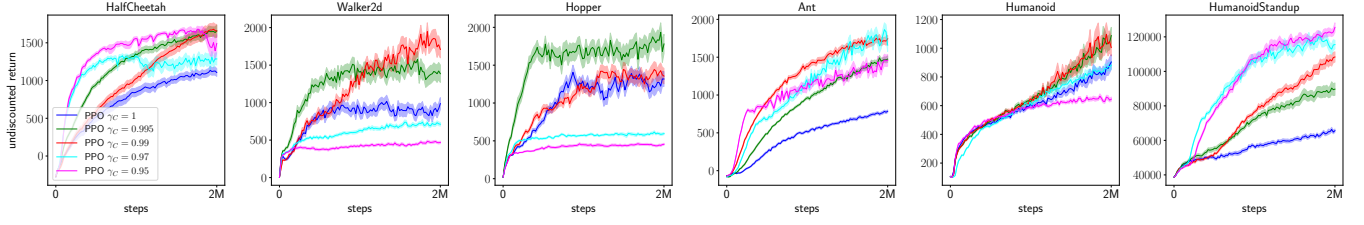


Figure 1: The default PPO implementation with different discount factors.

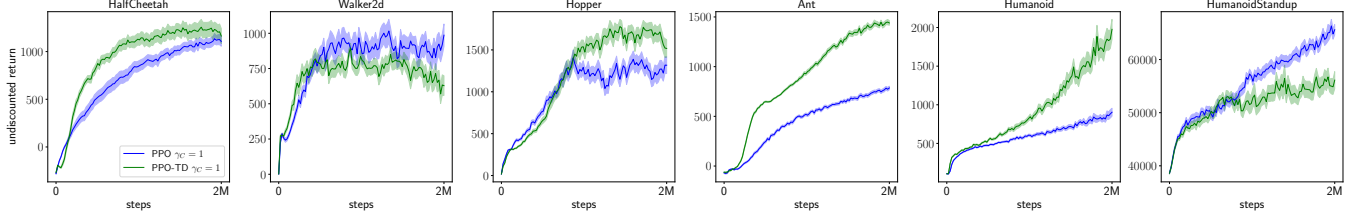


Figure 2: Comparison between PPO and PPO-TD when $\gamma_C = 1$.

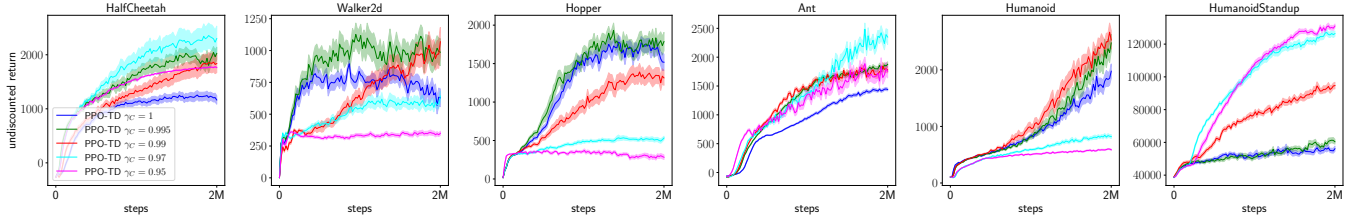


Figure 3: PPO-TD with different discount factors.

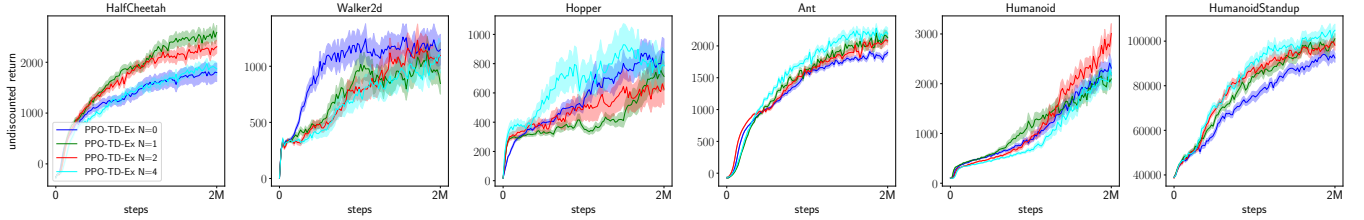


Figure 4: PPO-TD-Ex ($\gamma_C = 0.99$).

in 4 out of 6 tasks (Figure 5). This drop suggests that the quality of the critic \hat{v} , at least in terms of making prediction on untrained states $\{S_{t+1}^i\}_{1,\dots,N}$, is lower when $\gamma_C = 1$ is used than $\gamma_C < 1$. In other words, the generalization of \hat{v} becomes poorer when γ_C is increased from 0.99 to 1. The curves for PPO-TD-Ex ($\gamma_C = 0.995$) are a mixture of $\gamma_C = 0.99$ and $\gamma_C = 1$ and are provided in Figure 13 in the appendix. The limited generalization could imply that representation learning becomes harder when γ_C is increased. By representation learning, we refer to learning the lower layers (backbone) of a neural network. The last layer of the neural network is then interpreted as a linear function approximator whose features

are the output of the backbone. This interpretation of representation learning is widely used in the RL community, see, e.g., Chung et al. [10], Jaderberg et al. [19], Veeriah et al. [48].

In PPO-TD, the bootstrapping target for training $\hat{v}(S_t)$ is $R_{t+1} + \gamma_C \hat{v}(S_{t+1})$, where γ_C has two roles. First, it gates the randomness from S_{t+1} , which is the aforementioned variance control. Second, it affects the value function $v_\pi^{\gamma_C}$ that we want to approximate via changing the horizon of the policy evaluation problem, which could possibly affect the difficulty of learning a good estimate \hat{v} for $v_\pi^{\gamma_C}$ directly, not through the variance, which we refer to as *learnability control* (see, e.g., Laroché and van Seijen [26], Lehnert et al. [27], Romoff et al. [35]). Both roles can be responsible for the increased difficulty in representation learning when γ_C is increased. In the

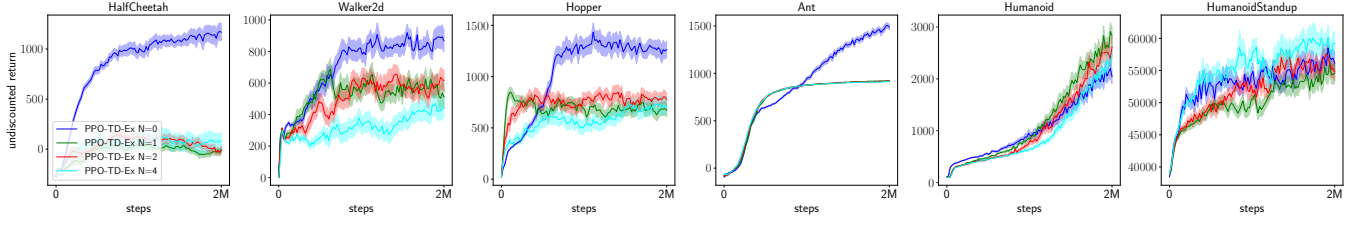


Figure 5: PPO-TD-Ex ($\gamma_c = 1$).

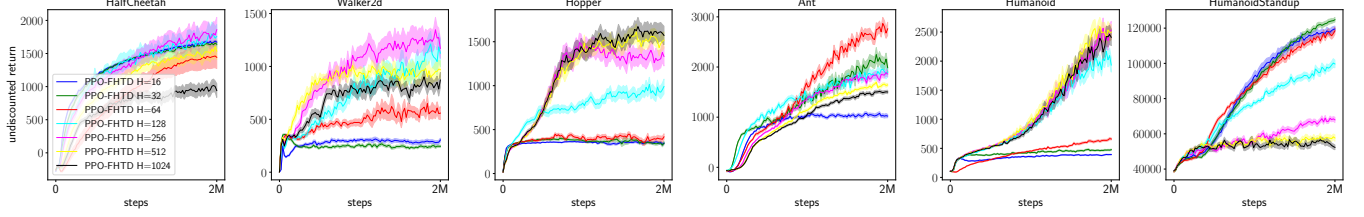


Figure 6: PPO-FHTD with the first parameterization. The best H and γ_c are used for each game.

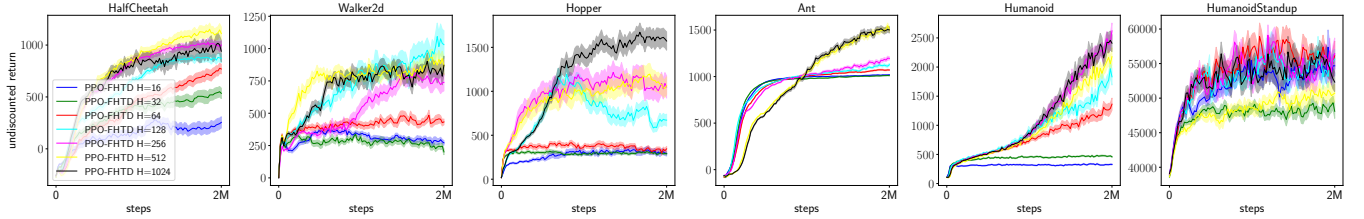


Figure 7: PPO-FHTD with the second parameterization.

rest of this section, we provide empirical evidence showing that the changed difficulty in representation learning, resulting directly from the changed horizon of the policy evaluation problem, is at play when using the $\gamma_c < 1$, which, together with the previously established bias-variance trade-off, suggests that a *bias-variance-representation trade-off* is at play when practitioners use $\gamma_c < 1$.

Bias-representation trade-off: To further disentangle the variance control effect and learnability control effect of γ_c , we use FHTD to train the critic in PPO, which we refer to as PPO-FHTD (Algorithm 4 in the appendix). PPO-FHTD always uses $\gamma_c = 1$ regardless of H . The critic update target in PPO-TD is $R_{t+1} + \gamma_c \hat{v}(S_{t+1})$, whose variance is

$$\begin{aligned} & \text{Var}(R_{t+1} + \gamma_c \hat{v}(S_{t+1}) | S_t) \\ &= \text{Var}(r(S_t) + \gamma_c \hat{v}(S_{t+1}) | S_t) \\ &= \gamma_c^2 \text{Var}(\hat{v}(S_{t+1}) | S_t). \end{aligned} \quad (5)$$

By contrast, the critic update target in PPO-FHTD for $\hat{v}^i(S_t)$ is $R_{t+1} + \hat{v}^{i-1}(S_{t+1})$, with variance:

$$\text{Var}(R_{t+1} + \hat{v}^{i-1}(S_{t+1}) | S_t) = \text{Var}(\hat{v}^{i-1}(S_{t+1}) | S_t). \quad (6)$$

On the one hand, manipulating H in FHTD changes the horizon of the policy evaluation problem, which corresponds to the role of learnability control of γ_c . On the other hand, manipulating H does not change the multiplier proceeding the variance term (c.f. (5)

and (6)) and thus separates variance control from the learnability control.

We test two parameterizations for PPO-FHTD to investigate representation learning. In the first parameterization, to learn v_π^H , we parameterize $\{v_\pi^i\}_{i=1,\dots,H}$ as H different heads over the same representation layer (backbone). In the second parameterization, we always learn $\{v_\pi^i\}_{i=1,\dots,1024}$ as 1024 different heads over the same representation layer, regardless of what H we are interested in. To approximate v_π^H , we then simply use the output of the H -th head. Figure 8 further illustrates the difference between the two parameterizations.

Figure 6 shows that with the first parameterization, the best H for PPO-FHTD is usually smaller than 1024. Figure 7, however, suggests that for the second parameterization, $H = 1024$ is almost always among the best choices of H . Comparing Figures 3 and 7 shows that the performance of PPO-FHTD ($H = 1024$) is close to the performance of PPO-TD ($\gamma_c = 1$) as expected, since for any $H \geq T_{\max} = 1000$, we always have $v_\pi^H(s) \equiv v_\pi^{\gamma=1}(s)$. This performance similarity suggests that learning $\{v_\pi^i\}_{i=1,\dots,1023}$ is not an additional overhead for the network in terms of learning $v_\pi^{H=1024}$, i.e., increasing H does not pose additional challenges in terms of network capacity. Then, comparing Figures 6 and 7, we conclude

⁴The trend that NRE decreases as α increases is merely an artifact from how we generate v_γ .

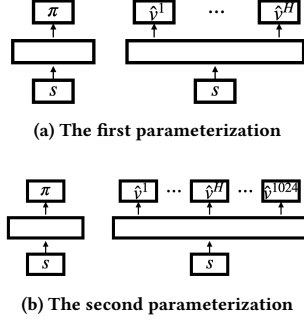


Figure 8: Two parameterization of PPO-FHTD

that in the tested domains, learning v_π^H with different H requires different representations. This suggests that we can interpret the results in Figure 6 as a *bias-representation trade-off*. Using a larger H is less biased but representation learning *may* become harder due to the longer policy evaluation horizon. Consequently, an intermediate H achieves the best performance in Figure 6. As reducing H cannot bring in advantages in representation learning under the second parameterization, the less biased H , *i.e.*, the larger H usually performs better in Figure 7. Overall, γ_c optimizes a *bias-representation trade-off* by changing the policy evaluation horizon H .

We further conjecture that representation learning may be harder for a longer horizon because the volume of all of good representations can become smaller. We provide a simulated example to support this. Consider policy evaluation on the simple Markov Reward Process (MRP) from Figure 10. We assume the reward for each transition is fixed, which is randomly generated in $[0, 1]$. Let $x_s \in \mathbb{R}^K$ be the feature vector for a state s ; we set its i -th component as $x_s[i] \doteq \tanh(\xi)$, where ξ is a random variable uniformly distributed in $[-2, 2]$. We choose this feature setup as we use \tanh as the activation function in our PPO. We use $X \in \mathbb{R}^{N \times K}$ to denote the feature matrix. To create state aliasing (McCallum [29]), which is common under function approximation, we first randomly split the N states into \mathcal{S}_1 and \mathcal{S}_2 such that $|\mathcal{S}_1| = \alpha N$ and $|\mathcal{S}_2| = (1 - \alpha)N$, where α is the proportion of states to be aliased. Then for every $s \in \mathcal{S}_1$, we randomly select an $\hat{s} \in \mathcal{S}_2$ and set $x_s \leftarrow x_{\hat{s}}$. Finally, we add Gaussian noise $\mathcal{N}(0, 0.1^2)$ to each element of X . We use $N = 100$ and $K = 30$ in our simulation and report the normalized representation error (NRE) as a function of γ . For a feature matrix X , the NRE is computed *analytically* as

$$\text{NRE}(\gamma) \doteq \frac{\min_w \|Xw - v_\gamma\|_2}{\|v_\gamma\|_2},$$

where v_γ is the *analytically* computed true value function of the MRP. We report the results in Figure 9, where each data point is averaged over 10^4 randomly generated feature matrices (X) and reward functions. In this MRP, the average representation error becomes larger as γ increases, which suggests that, in this MRP, the volume of good representations (*e.g.*, representations whose normalized representation error are smaller than some threshold) becomes smaller under a larger γ than that under a smaller γ .

Importantly, in this MRP experiment, we *compute all the quantities analytically so no variance is involved within a single trial*. Consequently, representation error is a property of v_γ itself. We report the unnormalized representation error in Figure 14 in the appendix, where the trend is much clearer.

Overall, though we do not claim that there is a monotonic relationship between the discount factor and the difficulty of representation learning, our empirical study suggests that representation learning is a key factor at play in the misuse of the discounting in actor-critic algorithms, beyond the widely recognized bias-variance trade-off.

4 OPTIMIZING THE DISCOUNTED OBJECTIVE (SCENARIO 2)

When our goal is to optimize the *discounted* objective $J_{\gamma < 1}(\pi)$, theoretically we should have the γ_A^t term in the actor update and use $\gamma_c < 1$. Practitioners, however, usually ignore this γ_A^t (*i.e.*, set $\gamma_A = 1$), introducing *bias* (see, *e.g.*, the default PPO, Algorithm 1 in the Appendix). By adding this missing γ_A^t term back (*i.e.*, setting $\gamma_A = \gamma < 1$), we end up with an unbiased implementation, which we refer to as DisPPO (Algorithm 5 in the Appendix). Figure 11, however, shows that even if we use the *discounted* return as the performance metric, the biased implementation of PPO still outperforms the theoretically grounded unbiased implementation DisPPO in some tasks.⁶ We propose to interpret the empirical advantages of PPO over DisPPO with Hypothesis 2. For all experiments in this section, we use $\gamma_c = \gamma < 1$.

An auxiliary task perspective: The biased policy update implementation of (2) ignoring γ_A^t can be decomposed into two parts as

$$\begin{aligned} & q_\pi^{\gamma_c}(S_t, A_t) \nabla_\theta \log \pi(A_t | S_t) \\ &= \gamma^t q_\pi^{\gamma_c}(S_t, A_t) \nabla_\theta \log \pi(A_t | S_t) \\ & \quad + (1 - \gamma^t) q_\pi^{\gamma_c}(S_t, A_t) \nabla_\theta \log \pi(A_t | S_t). \end{aligned}$$

We propose to interpret the *difference term* between the biased implementation $q_\pi^{\gamma_c}(S_t, A_t) \nabla_\theta \log \pi(A_t | S_t)$ and the theoretically grounded implementation $\gamma^t q_\pi^{\gamma_c}(S_t, A_t) \nabla_\theta \log \pi(A_t | S_t)$, *i.e.*, the $(1 - \gamma^t) q_\pi^{\gamma_c}(S_t, A_t) \nabla_\theta \log \pi(A_t | S_t)$ term, as the gradient of an auxiliary objective with a dynamic weighting $1 - \gamma^t$. Let

$$J_{s,\mu}(\pi) \doteq \sum_a \pi(a|s) q_\mu^\gamma(s, a),$$

we have

$$\nabla_\theta J_{s,\mu}(\pi)|_{\mu=\pi} = \mathbb{E}_{a \sim \pi(\cdot|s)} [q_\pi^\gamma(s, a) \nabla_\theta \log \pi(a|s)].$$

This objective changes every time step (through μ). Inspired by the decomposition, we augment PPO with this auxiliary task, yielding AuxPPO (Algorithm 6 in the appendix). In AuxPPO, we have two policies π and π' parameterized by θ and θ' respectively. The two policies are two heads over the same neural network backbone, where π is used for interaction with the environment and π' is the policy for the auxiliary task. AuxPPO optimizes θ and θ' simultaneously by considering the following joint loss

$$L(\theta, \theta') \doteq \sum_{t=0}^\infty \gamma^t L_t(\theta, \theta_{\text{old}}) + (1 - \gamma^t) L_t(\theta', \theta_{\text{old}}),$$

⁵See Section B.1 for more details about task selection.

⁶In this scenario, by a task we mean the combination of a game and a discount factor.

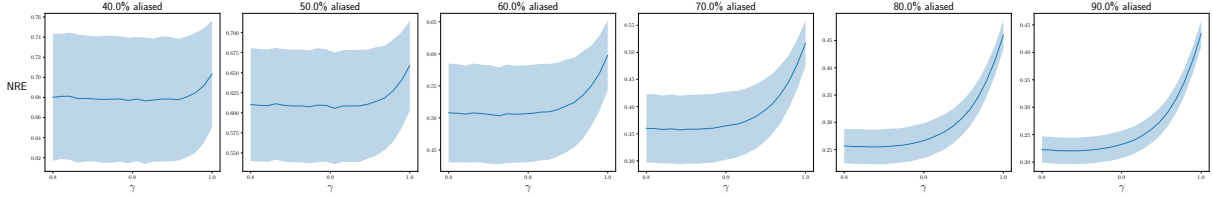


Figure 9: Normalized representation error as a function of the discount factor. Shaded regions indicate one standard derivation.

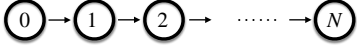


Figure 10: A simple MRP.

where S_t and A_t are obtained by executing $\pi_{\theta_{\text{old}}}$. We additionally synchronize θ' with θ periodically to avoid an off-policy learning issue. By contrast, the objectives for PPO and DisPPO are $\sum_{t=0}^{\infty} \gamma^t L_t(\theta, \theta_{\text{old}}) + (1 - \gamma^t) L_t(\theta, \theta_{\text{old}})$ and $\sum_{t=0}^{\infty} \gamma^t L_t(\theta, \theta_{\text{old}})$ respectively. Figure 12 further illustrates the architecture of AuxPPO.

Flipped rewards: Besides AuxPPO, we also design novel environments with flipped rewards to investigate Hypothesis 2. Recall we include the time step in the state, which allows us to create a new environment by simply defining a new reward function

$$r'(s, t) \doteq r(s) \mathbb{I}_{t \leq t_0} - r(s) \mathbb{I}_{t > t_0},$$

where \mathbb{I} is the indicator function. During an episode, within the first t_0 steps, this new environment is the same as the original one. After t_0 steps, the sign of the reward is flipped. We select t_0 such that γ^{t_0} is sufficiently small, e.g., we define $t_0 \doteq \min_t \{\gamma^t < 0.05\}$. With this criterion for selecting t_0 , the later transitions (i.e., transitions after t_0 steps) have little influence on the evaluation objective, the discounted return. Consequently, the later transitions affect the overall learning process mainly through representation learning. DisPPO rarely makes use of the later transitions due to the γ_A^t term in the gradient update. AuxPPO makes use of the later transitions only through representation learning (i.e., through the training of π'). PPO exploits the later transitions for representation learning and the later transitions also affect the control policy of PPO directly.

Results: When we consider the original environments, Figure 11 shows that in 8 out of 12 tasks, PPO outperforms DisPPO, even if the performance metric is the *discounted* episodic return. In all those 8 tasks, by using the difference term as an auxiliary task, AuxPPO is able to improve upon DisPPO. In 5 out of those 8 tasks, AuxPPO is able to roughly match the performance of PPO at the end of training. For $\gamma \in \{0.95, 0.93, 0.9\}$ in Ant, the improvement of AuxPPO is not clear and we conjecture that this is because the learning of the π -head (the control head) in AuxPPO is much slower than the learning of π in PPO due to the γ_C^t term. Overall, this suggests that the benefit of PPO over DisPPO comes mainly from representation learning.

When we consider the environments with flipped rewards, PPO is outperformed by DisPPO and AuxPPO by a large margin in 10 out of 12 tasks. The transitions after t_0 steps are not directly

relevant when the performance metric is the discounted return. However, learning on those transitions may still improve representation learning provided that those transitions are similar to the earlier transitions, which is the case in the original environments. PPO and AuxPPO, therefore, outperform DisPPO. However, when those transitions are much different from the earlier transitions, which is the case in the environments with flipped rewards, updating the control policy π_{θ} directly based on those transitions becomes distracting. DisPPO, therefore, outperforms PPO. Unlike PPO, AuxPPO does not update the control policy π_{θ} on later transitions directly. Provided that the network has enough capacity, the irrelevant transitions do not affect the control policy π_{θ} in AuxPPO much. The performance of AuxPPO is, therefore, similar to that of DisPPO.

To summarize, Figure 11 suggests that using $\gamma_A = 1$ is simply an *inductive bias* that *all transitions are equally important*. When this inductive bias is helpful for learning, $\gamma_A = 1$ implicitly implements auxiliary tasks thus improving representation learning and the overall performance. When this inductive bias is detrimental, however, $\gamma_A = 1$ can lead to significant performance drops. AuxPPO appears to be a safe choice that does not depend much on the correctness of this inductive bias.

5 RELATED WORK

The mismatch in actor-critic algorithm implementations has been previously studied. Thomas [45] focuses on the natural policy gradient setting and shows that the biased implementation ignoring γ_A^t can be interpreted as the gradient of the average reward objective under a strong assumption that the state distribution is independent of the policy. Nota and Thomas [31] prove that without this strong assumption, the biased implementation is *not* the gradient of any *stationary* objective. This does not contradict our auxiliary task perspective as our objective $J_{s, \mu}(\pi)$ changes at every time step. Nota and Thomas [31] further provide a counterexample showing that following the biased gradient can lead to a poorly performing policy w.r.t. both discounted and undiscounted objectives. Both Thomas [45] and Nota and Thomas [31], however, focus on *theoretical disadvantages* of the biased gradient and regard ignoring γ_A^t as the source of the bias. We instead regard the introduction of $\gamma_C < 1$ in the critic as the source of the bias in the undiscounted setting and investigate its *empirical advantages*, which are more relevant to practitioners. Moreover, our representation learning perspective for investigating this mismatch is to our knowledge novel. The concurrent work Tang et al. [44] regards the biased implementation with $\gamma_A = 1$ as a partial gradient. Tang et al. [44], however, do not

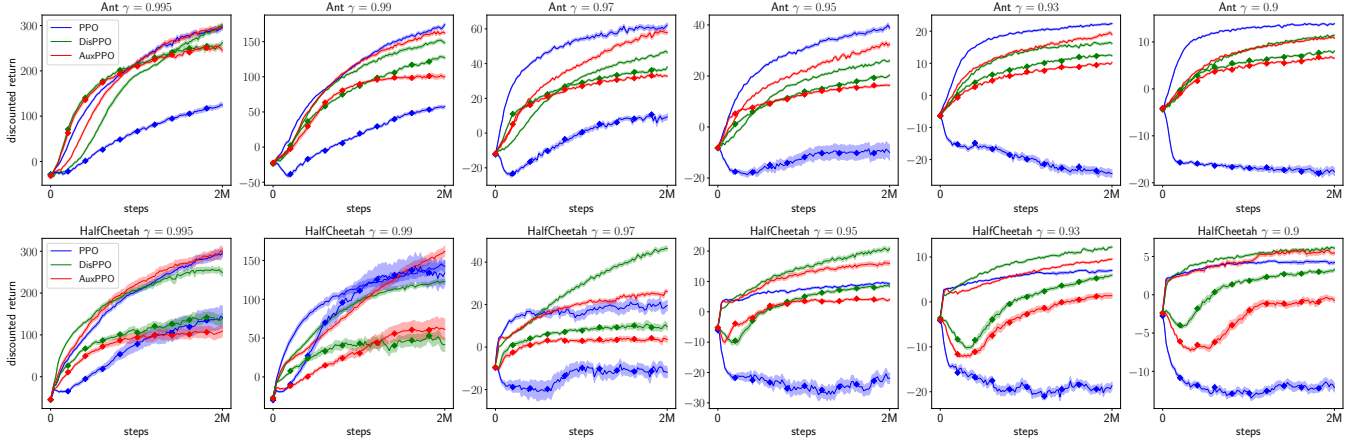


Figure 11: Curves without any marker are obtained in the original Ant / HalfCheetah. Diamond-marked curves are obtained in Ant / HalfCheetah with r' .⁵

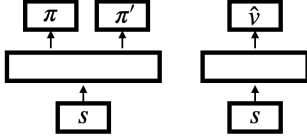


Figure 12: Architecture of AuxPPO

explain why this partial gradient can lead to empirical advantages over the full gradient. The concurrent work Laroche and Tachet [25] proves that in the second scenario, the biased setup can also converge to the optimal policy in the tabular setting, assuming we have access to the transition kernel and the true value function. Their results, however, heavily rely on the properties of the tabular setting and do not apply to the function approximation setting we consider.

Although we propose the *bias-variance-representation* trade-off, we do not claim that is all that γ affects. The discount factor also has many other effects (e.g., Amit et al. [3], Fedus et al. [14], Jiang et al. [20], Laroche et al. [24], Laroche and van Seijen [26], Lehnert et al. [27], Sutton [42], Van Seijen et al. [47]), the analysis of which we leave for future work. In Scenario 1, using $\gamma_C < 1$ helps reduce the variance. Variance reduction in RL itself is an active research area (see, e.g., Papini et al. [33], Xu et al. [53], Yuan et al. [54]). Investigating those variance reduction techniques with $\gamma_C = 1$ is another possibility for future work. Recently, Bengio et al. [6] study the effect of the bootstrapping parameter λ in TD(λ) in generalization. Our work studies the effect of the discount factor γ in representation learning in the context of the misuse of the discounting in actor-critic algorithms, sharing a similar spirit of Bengio et al. [6].

6 CONCLUSION

In this paper, we investigated the longstanding mismatch between theory and practice in actor-critic algorithms from a representation learning perspective. Although the theoretical understanding of policy gradient algorithms has recently advanced significantly (Agarwal et al. [2], Wu et al. [52]), this mismatch has drawn little attention. We proposed to understand this mismatch from a bias-representation trade-off perspective and an auxiliary task perspective for two different scenarios. We hope our empirical study can help practitioners understand actor-critic algorithms better and therefore design more efficient actor-critic algorithms in the setting of deep RL, where representation learning emerges as a major consideration, as well as draw more attention to the mismatch, which could enable the community to finally close this longstanding gap.

ACKNOWLEDGMENTS

We thank Geoffrey J. Gordon, Marc-Alexandre Cote, Bei Peng, and Dipendra Misra for the insightful discussion. Part of this work was done during SZ’s internship at Microsoft Research Montreal. SZ is also funded by the Engineering and Physical Sciences Research Council (EPSRC). This project has received funding from the European Research Council under the European Union’s Horizon 2020 research and innovation programme (grant agreement number 637713). Part of the experiments was made possible by a generous equipment grant from NVIDIA.

REFERENCES

- [1] Joshua Achiam. 2018. Spinning Up in Deep Reinforcement Learning. (2018).
- [2] Alekh Agarwal, Sham M Kakade, Jason D Lee, and Gaurav Mahajan. 2019. Optimality and approximation with policy gradient methods in markov decision processes. *arXiv preprint arXiv:1908.00261* (2019).
- [3] Ron Amit, Ron Meir, and Kamil Ciosek. 2020. Discount Factor as a Regularizer in Reinforcement Learning. *arXiv preprint arXiv:2007.02040* (2020).
- [4] Marcin Andrychowicz, Anton Raichuk, Piotr Stańczyk, Manu Orsini, Sertan Girgin, Raphael Marinier, Léonard Hussenot, Matthieu Geist, Olivier Pietquin, Marcin Michalski, et al. 2020. What Matters In On-Policy Reinforcement Learning? A Large-Scale Empirical Study. *arXiv preprint arXiv:2006.05990* (2020).
- [5] M. G. Bellemare, Y. Naddaf, J. Veness, and M. Bowling. 2013. The Arcade Learning Environment: An Evaluation Platform for General Agents. *Journal of Artificial Intelligence Research* 47 (jun 2013), 253–279.

- [6] Emmanuel Bengio, Joelle Pineau, and Doina Precup. 2020. Interference and Generalization in Temporal Difference Learning. *arXiv preprint arXiv:2003.06350* (2020).
- [7] Dimitri P Bertsekas and John N Tsitsiklis. 1996. *Neuro-Dynamic Programming*. Athena Scientific Belmont, MA.
- [8] Greg Brockman, Vicki Cheung, Ludwig Pettersson, Jonas Schneider, John Schulman, Jie Tang, and Wojciech Zaremba. 2016. Openai gym. *arXiv preprint arXiv:1606.01540* (2016).
- [9] Itai Caspi, Gal Leibovich, Gal Novik, and Shadi Endrawis. 2017. Reinforcement Learning Coach. <https://doi.org/10.5281/zenodo.1134899>
- [10] Wesley Chung, Somjit Nath, Ajin Joseph, and Martha White. 2018. Two-timescale networks for nonlinear value function approximation. In *International Conference on Learning Representations*.
- [11] Kristopher De Asis, Alan Chan, Silviu Pitis, Richard S Sutton, and Daniel Graves. 2019. Fixed-horizon temporal difference methods for stable reinforcement learning. *arXiv preprint arXiv:1909.03906* (2019).
- [12] Prafulla Dhariwal, Christopher Hesse, Oleg Klimov, Alex Nichol, Matthias Plappert, Alec Radford, John Schulman, Szymon Sidor, Yuhui Wu, and Peter Zhokhov. 2017. OpenAI Baselines. <https://github.com/openai/baselines>.
- [13] Logan Engstrom, Andrew Ilyas, Shibani Santurkar, Dimitris Tsipras, Firdaus Janoos, Larry Rudolph, and Aleksander Madry. 2019. Implementation Matters in Deep RL: A Case Study on PPO and TRPO. In *International Conference on Learning Representations*.
- [14] William Fedus, Carles Gelada, Yoshua Bengio, Marc G Bellemare, and Hugo Larochelle. 2019. Hyperbolic discounting and learning over multiple horizons. *arXiv preprint arXiv:1902.06865* (2019).
- [15] Scott Fujimoto, Herke van Hoof, and David Meger. 2018. Addressing function approximation error in actor-critic methods. *arXiv preprint arXiv:1802.09477* (2018).
- [16] Tuomas Haarnoja, Aurick Zhou, Pieter Abbeel, and Sergey Levine. 2018. Soft actor-critic: Off-policy maximum entropy deep reinforcement learning with a stochastic actor. *arXiv preprint arXiv:1801.01290* (2018).
- [17] Peter Henderson, Riashat Islam, Philip Bachman, Joelle Pineau, Doina Precup, and David Meger. 2017. Deep reinforcement learning that matters. *arXiv preprint arXiv:1709.06560* (2017).
- [18] Andrew Ilyas, Logan Engstrom, Shibani Santurkar, Dimitris Tsipras, Firdaus Janoos, Larry Rudolph, and Aleksander Madry. 2018. A Closer Look at Deep Policy Gradients. *arXiv preprint arXiv:1811.02553* (2018).
- [19] Max Jaderberg, Volodymyr Mnih, Wojciech Marian Czarnecki, Tom Schaul, Joel Z Leibo, David Silver, and Koray Kavukcuoglu. 2016. Reinforcement learning with unsupervised auxiliary tasks. *arXiv preprint arXiv:1611.05397* (2016).
- [20] Nan Jiang, Satinder P Singh, and Ambuj Tewari. 2016. On Structural Properties of MDPs that Bound Loss Due to Shallow Planning. In *IJCAI*.
- [21] Diederik P Kingma and Jimmy Ba. 2014. Adam: A method for stochastic optimization. *arXiv preprint arXiv:1412.6980* (2014).
- [22] Vijay R Konda. 2002. *Actor-critic algorithms*. Ph.D. Dissertation. Massachusetts Institute of Technology.
- [23] Ilya Kostrikov. 2018. PyTorch Implementations of Reinforcement Learning Algorithms. <https://github.com/ikostrikov/pytorch-a2c-ppo-acktr-gail>.
- [24] Romain Laroche, Mehdi Fatemi, Joshua Romoff, and Harm van Seijen. 2017. Multi-advisor reinforcement learning. *arXiv preprint arXiv:1704.00756* (2017).
- [25] Romain Laroche and Remi Tachet. 2021. Dr Jekyll and Mr Hyde: the Strange Case of Off-Policy Policy Updates. *arXiv preprint arXiv:2109.14727* (2021).
- [26] Romain Laroche and Harm van Seijen. 2018. In reinforcement learning, all objective functions are not equal. (2018).
- [27] Lucas Lehnert, Romain Laroche, and Harm van Seijen. 2018. On value function representation of long horizon problems. In *AAAI Conference on Artificial Intelligence*.
- [28] Eric Liang, Richard Liaw, Robert Nishihara, Philipp Moritz, Roy Fox, Ken Goldberg, Joseph Gonzalez, Michael Jordan, and Ion Stoica. 2018. RLlib: Abstractions for distributed reinforcement learning. In *International Conference on Machine Learning*.
- [29] R McCallum. 1997. *Reinforcement learning with selective perception and hidden state*. Ph.D. Dissertation.
- [30] Volodymyr Mnih, Adria Puigdomenech Badia, Mehdi Mirza, Alex Graves, Timothy Lillicrap, Tim Harley, David Silver, and Koray Kavukcuoglu. 2016. Asynchronous methods for deep reinforcement learning. In *Proceedings of the 33rd International Conference on Machine Learning*.
- [31] Chris Notia and Philip S. Thomas. 2020. Is the Policy Gradient a Gradient?, In *Proceedings of the 19th International Conference on Autonomous Agents and Multiagent Systems*. CoRR.
- [32] OpenAI. 2018. OpenAI Five. <https://openai.com/five/>.
- [33] Matteo Papini, Damiano Binaghi, Giuseppe Canonaco, Matteo Pirodda, and Marcello Restelli. 2018. Stochastic variance-reduced policy gradient. *arXiv preprint arXiv:1806.05618* (2018).
- [34] Fabio Pardo, Arash Tavakoli, Vitaly Levnik, and Petar Kormushev. 2018. Time limits in reinforcement learning. In *International Conference on Machine Learning*.
- [35] Joshua Romoff, Peter Henderson, Ahmed Touati, Emma Brunskill, Joelle Pineau, and Yann Ollivier. 2019. Separating value functions across time-scales. *arXiv preprint arXiv:1902.01883* (2019).
- [36] John Schulman, Sergey Levine, Pieter Abbeel, Michael Jordan, and Philipp Moritz. 2015. Trust region policy optimization. In *Proceedings of the 32nd International Conference on Machine Learning*.
- [37] John Schulman, Philipp Moritz, Sergey Levine, Michael Jordan, and Pieter Abbeel. 2015. High-dimensional continuous control using generalized advantage estimation. *arXiv preprint arXiv:1506.02438* (2015).
- [38] John Schulman, Filip Wolski, Prafulla Dhariwal, Alec Radford, and Oleg Klimov. 2017. Proximal policy optimization algorithms. *arXiv preprint arXiv:1707.06347* (2017).
- [39] David Silver, Aja Huang, Chris J Maddison, Arthur Guez, Laurent Sifre, George Van Den Driessche, Julian Schrittwieser, Ioannis Antonoglou, Veda Panneershelvam, Marc Lanctot, et al. 2016. Mastering the game of Go with deep neural networks and tree search. *Nature* (2016).
- [40] Adam Stooke and Pieter Abbeel. 2019. rlpyt: A research code base for deep reinforcement learning in pytorch. *arXiv preprint arXiv:1909.01500* (2019).
- [41] Richard S Sutton. 1988. Learning to predict by the methods of temporal differences. *Machine Learning* (1988).
- [42] Richard S Sutton. 1995. TD models: Modeling the world at a mixture of time scales. In *Machine Learning Proceedings 1995*. Elsevier.
- [43] Richard S Sutton, David A McAllester, Satinder P Singh, and Yishay Mansour. 2000. Policy gradient methods for reinforcement learning with function approximation. In *Advances in Neural Information Processing Systems*.
- [44] Yunhao Tang, Mark Rowland, Rémi Munos, and Michal Valko. 2021. Taylor Expansion of Discount Factors. *arXiv preprint arXiv:2106.06170* (2021).
- [45] Philip Thomas. 2014. Bias in natural actor-critic algorithms. In *Proceedings of the 31st International Conference on Machine Learning*.
- [46] Emanuel Todorov, Tom Erez, and Yuval Tassa. 2012. Mujoco: A physics engine for model-based control. In *2012 IEEE/RSJ International Conference on Intelligent Robots and Systems*.
- [47] Harm Van Seijen, Mehdi Fatemi, and Arash Tavakoli. 2019. Using a Logarithmic Mapping to Enable Lower Discount Factors in Reinforcement Learning. In *Advances in Neural Information Processing Systems*.
- [48] Vivek Veeriah, Matteo Hessel, Zhongwen Xu, Janarthanan Rajendran, Richard L Lewis, Junhyuk Oh, Hado P van Hasselt, David Silver, and Satinder Singh. 2019. Discovery of useful questions as auxiliary tasks. In *Advances in Neural Information Processing Systems*.
- [49] Arthur F Veinott. 1969. Discrete dynamic programming with sensitive discount optimality criteria. *The Annals of Mathematical Statistics* (1969).
- [50] Martin L Weitzman. 2001. Gamma discounting. *American Economic Review* (2001).
- [51] Ronald J Williams. 1992. Simple statistical gradient-following algorithms for connectionist reinforcement learning. *Machine learning* (1992).
- [52] Yue Wu, Weitong Zhang, Pan Xu, and Quanquan Gu. 2020. A Finite Time Analysis of Two Time-Scale Actor Critic Methods. *arXiv preprint arXiv:2005.01350* (2020).
- [53] Pan Xu, Felicia Gao, and Quanquan Gu. 2019. Sample efficient policy gradient methods with recursive variance reduction. *arXiv preprint arXiv:1909.08610* (2019).
- [54] Huizhuo Yuan, Xiangru Lian, Ji Liu, and Yuren Zhou. 2020. Stochastic Recursive Momentum for Policy Gradient Methods. *arXiv preprint arXiv:2003.04302* (2020).
- [55] Shangdong Zhang. 2018. Modularized Implementation of Deep RL Algorithms in PyTorch. <https://github.com/ShangdongZhang/DeepRL>.

A PROOF OF LEMMA 2.2

PROOF. The proof is based on Appendix B in Schulman et al. [36], where perturbation theory is used to prove the performance improvement bound (Lemma 2.1). To simplify notation, we use a vector and a function interchangeably, *i.e.*, we also use r and μ_0 to denote the reward vector and the initial distribution vector. $J(\pi)$ and $d_\pi(s)$ are shorthand for $J_\gamma(\pi)$ and $d_\pi^\gamma(s)$ with $\gamma = 1$. All vectors are *column* vectors.

Let \mathcal{S}^+ be the set of states excluding s^∞ , *i.e.*, $\mathcal{S}^+ \doteq \mathcal{S}/\{s^\infty\}$, we define $P_\pi \in \mathbb{R}^{|\mathcal{S}^+| \times |\mathcal{S}^+|}$ such that $P_\pi(s, s') \doteq \sum_a \pi(a|s)p(s'|s, a)$. Let $G \doteq \sum_{t=0}^{\infty} P_\pi^t$. According to standard Markov chain theories, $G(s, s')$ is the expected number of times that s' is visited before s^∞ is hit given $S_0 = s$. $T_{\max} < \infty$ implies that G is well-defined and we have $G = (I - P_\pi)^{-1}$. Moreover, $T_{\max} < \infty$ also implies $\forall s, \sum_{s'} G(s, s') \leq T_{\max}$, *i.e.*, $\|G\|_\infty \leq T_{\max}$. We have $J(\pi) = \mu_0^\top Gr$.

Let $G' \doteq (I - P_{\pi'})^{-1}$, we have

$$J(\pi') - J(\pi) = \mu_0^\top (G' - G)r.$$

Let $\Delta \doteq P_{\pi'} - P_\pi$, we have

$$G'^{-1} - G^{-1} = -\Delta,$$

Left multiply by G' and right multiply by G ,

$$\begin{aligned} G - G' &= -G' \Delta G, \\ G' &= G + G' \Delta G \quad (\text{Expanding } G' \text{ in RHS recursively}) \\ &= G + G \Delta G + G' \Delta G \Delta G. \end{aligned}$$

So we have

$$J(\pi') - J(\pi) = \mu_0^\top G \Delta Gr + \mu_0^\top G' \Delta G \Delta Gr.$$

It is easy to see $\mu_0^\top G = d_\pi^\top$ and $Gr = v_\pi$. So

$$\begin{aligned} \mu_0^\top G \Delta Gr &= d_\pi^\top \Delta v_\pi \\ &= \sum_s d_\pi(s) \sum_{s'} \left(\sum_a \pi'(a|s)p(s'|s, a) - \sum_a \pi(a|s)p(s'|s, a) \right) v_\pi(s') \\ &= \sum_s d_\pi(s) \sum_a (\pi'(a|s) - \pi(a|s)) \sum_{s'} p(s'|s, a) v_\pi(s') \\ &= \sum_s d_\pi(s) \sum_a (\pi'(a|s) - \pi(a|s)) \left(r(s) + \sum_{s'} p(s'|s, a) v_\pi(s') - v_\pi(s) \right) \\ &\quad (\sum_a (\pi'(a|s) - \pi(a|s)) f(s) = 0 \text{ holds for any } f \text{ that depends only on } s) \\ &= \sum_s d_\pi(s) \sum_a \pi'(a|s) \text{Adv}_\pi(s, a). \end{aligned}$$

($\sum_a \pi(a|s) \text{Adv}_\pi(s, a) = 0$ by Bellman equation)

We now bound $\mu_0^\top G' \Delta G \Delta Gr$. First,

$$\begin{aligned} |(\Delta Gr)(s)| &= \left| \sum_{s'} \left(\sum_a \pi'(a|s) - \pi(a|s) \right) p(s'|s, a) v_\pi(s') \right| \\ &= \left| \sum_a \left(\pi'(a|s) - \pi(a|s) \right) \left(r(s) + \sum_{s'} p(s'|s, a) v_\pi(s') - v_\pi(s) \right) \right| \\ &= \left| \sum_a \left(\pi'(a|s) - \pi(a|s) \right) \text{Adv}_\pi(s, a) \right| \\ &\leq 2 \max_s D_{TV}(\pi'(\cdot|s), \pi(\cdot|s)) \max_{s,a} |\text{Adv}_\pi(s, a)|, \end{aligned}$$

where D_{TV} is the total variation distance. So

$$\|\Delta Gr\|_\infty \leq 2 \max_s D_{TV}(\pi'(\cdot|s), \pi(\cdot|s)) \max_{s,a} |\text{Adv}_\pi(s, a)|.$$

Moreover, for any vector x ,

$$\begin{aligned} |(\Delta x)(s)| &\leq 2 \max_s D_{TV}(\pi'(\cdot|s), \pi(\cdot|s)) \|x\|_\infty, \\ \|\Delta x\|_\infty &\leq 2 \max_s D_{TV}(\pi'(\cdot|s), \pi(\cdot|s)) \|x\|_\infty. \end{aligned}$$

So

$$\begin{aligned}
\|\Delta\|_\infty &\leq 2 \max_s D_{TV}(\pi'(\cdot|s), \pi(\cdot|s)), \\
|\mu_0^\top G' \Delta G \Delta G r| &\leq \|\mu_0^\top\|_1 \|G'\|_\infty \|\Delta\|_\infty \|G\|_\infty \|\Delta G r\|_\infty \\
&\leq 4 T_{\max}^2 \max_s D_{TV}^2(\pi'(\cdot|s), \pi(\cdot|s)) \max_{s,a} |\text{Adv}_\pi(s, a)| \\
&\leq 4 T_{\max}^2 \max_s D_{KL}(\pi(\cdot|s) \|\pi'(\cdot|s)) \max_{s,a} |\text{Adv}_\pi(s, a)|,
\end{aligned}$$

which completes the proof. \square

Note this perturbation-based proof of Lemma 2.2 holds only for $r : \mathcal{S} \rightarrow \mathbb{R}$. For $r : \mathcal{S} \times \mathcal{A} \rightarrow \mathbb{R}$, we can turn to the coupling-based proof as Schulman et al. [36], which, however, complicates the presentation and deviates from the main purpose of this paper. We, therefore, leave it for future work.

B EXPERIMENT DETAILS

We conducted our experiments on an Nvidia DGX-1 with PyTorch, though we do not use the GPUs there.

B.1 Methodology

We use HalfCheetah, Walker, Hopper, Ant, Humanoid, and HumanoidStandup as our benchmarks. We exclude other tasks as we find PPO plateaus quickly there. The tasks we consider have a hard time limit of 1000. Following Pardo et al. [34], we add time step information into the state, *i.e.*, there is an additional scalar $t/1000$ in the observation vector. Following Achiam [1], we estimate the KL divergence between the current policy θ and the sampling policy θ_{old} when optimizing the loss (3). When the estimated KL divergence is greater than a threshold, we stop updating the actor and update only the critic with current data. We use Adam (Kingma and Ba [21]) as the optimizer and perform grid search for the initial learning rates of Adam optimizers. Let α_A and $\alpha_C \doteq \beta \alpha_A$ be the learning rates for the actor and critic respectively. For each experiment unit (*i.e.* an algorithmic configuration and a task, *c.f.* a curve in a figure), we tune $\alpha_A \in \{0.125, 0.25, 0.5, 1, 2\} \times 3 \cdot 10^{-4}$ and $\beta \in \{1, 3\}$ with grid search with 3 independent runs maximizing the average return of the last 100 training episodes. In particular, $\alpha_A = 3 \cdot 10^{-4}$ and $\beta = 3$ is roughly the default learning rates for the PPO implementation in Achiam [1]. Overall, we find after removing GAE, smaller learning rates are preferred.

In the discounted setting, we consider only Ant, HalfCheetah and their variants. For Walker2d, Hopper, and Humanoid, we find the average episode length of all algorithms are smaller than t_0 , *i.e.*, the flipped reward rarely takes effects. For HumanoidStandup, the scale of the reward is too large. To summarize, other four environments are not well-suited for the purpose of our empirical study.

B.2 Algorithm Details

The pseudocode of all implemented algorithms are provide in Algorithms 1 - 6. For hyperparameters that are not included in the grid search, we use the same value as Achiam [1], Dhariwal et al. [12]. In particular, for the rollout length, we set $K = 2048$. For the optimization epochs, we set $K_{\text{opt}} = 320$. For the minibatch size, we set $B = 64$. For the maximum KL divergence, we set $KL_{\text{target}} = 0.01$. We clip $\frac{\pi_\theta(a|s)}{\pi_{\theta_{\text{old}}}(a|s)}$ into $[-0.2, 0.2]$.

We use two-hidden-layer neural networks for function approximation. Each hidden layer has 64 hidden units and a tanh activation function. The output layer of the actor network has a tanh activation function and is interpreted as the mean of an isotropic Gaussian distribution, whose standard derivation is a global state-independent variable as suggested by Schulman et al. [36].

Algorithm 1: PPO

Input:

θ, ψ : parameters of π, \hat{v} ;
 α_A, α_C : Initial learning rates of the Adam optimizers for θ, ψ ;
 K, K_{opt}, B : rollout length, number of optimization epochs, and minibatch size;
 KL_{target} : maximum KL divergence threshold

;

$S_0 \sim \mu_0$

while *True* **do**

 Initialize a buffer M ;

$\theta_{old} \leftarrow \theta$;

for $i = 0, \dots, K - 1$ **do**

$A_i \sim \pi_{\theta_{old}}(\cdot|S_i)$;

 Execute A_i , get R_{i+1}, S_{i+1} ;

if S_{i+1} is a terminal state **then**

$m_i \leftarrow 0, S_{i+1} \sim \mu_0$

else

$m_i \leftarrow 1$

end

end

$G_K \leftarrow \hat{v}(S_K)$;

for $i = K - 1, \dots, 0$ **do**

$G_i \leftarrow R_{i+1} + \gamma_C m_i G_{i+1}$;

$\text{Adv}_i \leftarrow R_{i+1} + \gamma_C m_i \hat{v}_\psi(S_{i+1}) - \hat{v}_\psi(S_i)$;

 Store $(S_i, A_i, G_i, \text{Adv}_i)$ in M ;

end

Normalize Adv_i in M as $\text{Adv}_i \leftarrow \frac{\text{Adv}_i - \text{mean}(\{\text{Adv}_i\})}{\text{std}(\{\text{Adv}_i\})}$;

for $o = 1, \dots, K_{opt}$ **do**

 Sample a minibatch $\{(S_i, A_i, G_i, \text{Adv}_i)\}_{i=1, \dots, B}$ from M ;

$L(\psi) \leftarrow \frac{1}{2B} \sum_{i=1}^B (\hat{v}_\psi(S_i) - G_i)^2$ /* No gradient through G_i */

$L(\theta) \leftarrow \frac{1}{B} \sum_{i=1}^B \min\{\frac{\pi_\theta(A_i|S_i)}{\pi_{\theta_{old}}(A_i|S_i)} \text{Adv}_i, \text{clip}(\frac{\pi_\theta(A_i|S_i)}{\pi_{\theta_{old}}(A_i|S_i)}) \text{Adv}_i\}$;

 Perform one gradient update to ψ minimizing $L(\psi)$ with Adam;

if $\frac{1}{B} \sum_{i=1}^B \log \pi_{\theta_{old}}(A_i|S_i) - \log \pi_\theta(A_i|S_i) < KL_{target}$ **then**

 Perform one gradient update to θ maximizing $L(\theta)$ with Adam;

end

end**end**

C ADDITIONAL EXPERIMENTAL RESULTS

Figure 13 shows how PPO-TD-Ex ($\gamma_C = 0.995$) reacts to the increase of N . Figure 14 shows the unnormalized representation error in the MRP experiment. Figure 15 shows the average episode length for the Ant environment in the discounted setting. For HalfCheetah, it is always 1000.

D LARGER VERSION OF FIGURES

Algorithm 2: PPO-TD

Input: θ, ψ : parameters of π, \hat{v} ; α_A, α_C : Initial learning rates of the Adam optimizers for θ, ψ ; K, K_{opt}, B : rollout length, number of optimization epochs, and minibatch size; KL_{target} : maximum KL divergence threshold

;

 $S_0 \sim \mu_0$ **while** *True* **do** Initialize a buffer M ; $\theta_{old} \leftarrow \theta$; **for** $i = 0, \dots, K - 1$ **do** $A_i \sim \pi_{\theta_{old}}(\cdot|S_i)$; Execute A_i , get R_{i+1}, S_{i+1} ; **if** S_{i+1} is a terminal state **then** $m_i \leftarrow 0, S_{i+1} \sim \mu_0$ **else** $m_i \leftarrow 1$ **end** **end** **for** $i = K - 1, \dots, 0$ **do** $\text{Adv}_i \leftarrow R_{i+1} + \gamma_C m_i \hat{v}_\psi(S_{i+1}) - \hat{v}_\psi(S_i)$; $S'_i \leftarrow S_{i+1}, r_i \leftarrow R_{i+1}$; Store $(S_i, A_i, m_i, r_i, S'_i, \text{Adv}_i)$ in M ; **end** Normalize Adv_i in M as $\text{Adv}_i \leftarrow \frac{\text{Adv}_i - \text{mean}(\{\text{Adv}_i\})}{\text{std}(\{\text{Adv}_i\})}$; **for** $o = 1, \dots, K_{opt}$ **do** Sample a minibatch $\{(S_i, A_i, m_i, r_i, S'_i, \text{Adv}_i)\}_{i=1, \dots, B}$ from M ; $y_i \leftarrow r_i + \gamma_C m_i \hat{v}_\psi(S'_i)$; $L(\psi) \leftarrow \frac{1}{2B} \sum_{i=1}^B (\hat{v}_\psi(S_i) - y_i)^2$ /* No gradient through y_i */ $L(\theta) \leftarrow \frac{1}{B} \sum_{i=1}^B \min\{\frac{\pi_\theta(A_i|S_i)}{\pi_{\theta_{old}}(A_i|S_i)} \text{Adv}_i, \text{clip}(\frac{\pi_\theta(A_i|S_i)}{\pi_{\theta_{old}}(A_i|S_i)}) \text{Adv}_i\}$; Perform one gradient update to ψ minimizing $L(\psi)$ with Adam; **if** $\frac{1}{B} \sum_{i=1}^B \log \pi_{\theta_{old}}(A_i|S_i) - \log \pi_\theta(A_i|S_i) < KL_{target}$ **then** Perform one gradient update to θ maximizing $L(\theta)$ with Adam; **end** **end****end**

Algorithm 3: PPO-TD-Ex

Input:

θ, ψ : parameters of π, \hat{v} ;
 α_A, α_C : Initial learning rates of the Adam optimizers for θ, ψ ;
 K, K_{opt}, B : rollout length, number of optimization epochs, and minibatch size;
 KL_{target} : maximum KL divergence threshold ;
 N : number of extra transitions ;
 p, r : transition kernel and reward function of the oracle
;
 $S_0 \sim \mu_0$

while *True* **do**

Initialize a buffer M ;

$\theta_{old} \leftarrow \theta$;

for $i = 0, \dots, K - 1$ **do****for** $j = 0, \dots, N$ **do**

$A_i^j \sim \pi_{\theta_{old}}(\cdot | S_i), R_{i+1}^j \leftarrow r(S_i, A_i^j), S_{i+1}^j \sim p(\cdot | S_i, A_i^j)$;

if S_{i+1}^j *is a terminal state* **then**

$m_i^j \leftarrow 0, S_{i+1}^j \sim \mu_0$

else

$m_i^j \leftarrow 1$

end

end

$S_{i+1} \leftarrow S_{i+1}^0$

end**for** $i = K - 1, \dots, 0$ **do**

$\text{Adv}_i \leftarrow R_{i+1}^0 + m_i^0 \hat{v}_\psi(S_{i+1}^0) - \hat{v}_\psi(S_i^0)$;

for $j = 0, \dots, N$ **do**

$S_i'^j \leftarrow S_{i+1}^j$

end

Store $(\{S_i^j, A_i^j, m_i^j, r_i^j, S_i'^j\}_{j=0, \dots, N}, \text{Adv}_i)$ in M ;

end

Normalize Adv_i in M as $\text{Adv}_i \leftarrow \frac{\text{Adv}_i - \text{mean}(\{\text{Adv}_i\})}{\text{std}(\{\text{Adv}_i\})}$;

for $o = 1, \dots, K_{opt}$ **do**

Sample a minibatch $\{(\{S_i^j, A_i^j, m_i^j, r_i^j, S_i'^j\}_{j=0, \dots, N}, \text{Adv}_i)\}_{i=1, \dots, B}$ from M ;

$y_i \leftarrow \frac{1}{N+1} \sum_{j=0}^N r_i^j + \gamma \mathbb{E} m_i^j \hat{v}_\psi(S_i'^j)$;

$L(\psi) \leftarrow \frac{1}{2B} \sum_{i=1}^B (\hat{v}_\psi(S_i^0) - y_i)^2$ /* No gradient through y_i */

$L(\theta) \leftarrow \frac{1}{B} \sum_{i=1}^B \min\{\frac{\pi_\theta(A_i^0 | S_i^0)}{\pi_{\theta_{old}}(A_i^0 | S_i^0)} \text{Adv}_i, \text{clip}(\frac{\pi_\theta(A_i^0 | S_i^0)}{\pi_{\theta_{old}}(A_i^0 | S_i^0)}) \text{Adv}_i\}$;

Perform one gradient update to ψ minimizing $L(\psi)$ with Adam;

if $\frac{1}{B} \sum_{i=1}^B \log \pi_{\theta_{old}}(A_i^0 | S_i^0) - \log \pi_\theta(A_i^0 | S_i^0) < KL_{target}$ **then**

 Perform one gradient update to θ maximizing $L(\theta)$ with Adam;

end

end**end**

Algorithm 4: PPO-FHTD

Input:

θ, ψ : parameters of $\pi, \{\hat{v}^j\}_{j=1,\dots,H}$;
 α_A, α_C : Initial learning rates of the Adam optimizers for θ, ψ ;
 K, K_{opt}, B : rollout length, number of optimization epochs, and minibatch size;
 KL_{target} : maximum KL divergence threshold

;

$S_0 \sim \mu_0$

while *True* **do**

 Initialize a buffer M ;

$\theta_{old} \leftarrow \theta$;

for $i = 0, \dots, K - 1$ **do**

$A_i \sim \pi_{\theta_{old}}(\cdot|S_i)$;

 Execute A_i , get R_{i+1}, S_{i+1} ;

if S_{i+1} is a terminal state **then**

$m_i \leftarrow 0, S_{i+1} \sim \mu_0$

else

$m_i \leftarrow 1$

end

end**for** $i = K - 1, \dots, 0$ **do**

$\text{Adv}_i \leftarrow R_{i+1} + m_i \hat{v}_{\psi}^H(S_{i+1}) - \hat{v}_{\psi}^H(S_i)$;

$S'_i \leftarrow S_{i+1}, r_i \leftarrow R_{i+1}$;

 Store $(S_i, A_i, m_i, r_i, S'_i, \text{Adv}_i)$ in M ;

end

Normalize Adv_i in M as $\text{Adv}_i \leftarrow \frac{\text{Adv}_i - \text{mean}(\{\text{Adv}_i\})}{\text{std}(\{\text{Adv}_i\})}$;

for $o = 1, \dots, K_{opt}$ **do**

 Sample a minibatch $\{(S_i, A_i, m_i, r_i, S'_i, \text{Adv}_i)\}_{i=1,\dots,B}$ from M ;

for $j = 1, \dots, H$ **do**

$y_i^j \leftarrow r_i + m_i \hat{v}_{\psi}^{j-1}(S'_i)$ $\text{/* } \hat{v}^0(S'_i) \equiv 0$ */

end

$L(\psi) \leftarrow \frac{1}{2B} \sum_{i=1}^B \sum_{j=1}^H (\hat{v}_{\psi}^j(S_i) - y_i^j)^2$ $\text{/* No gradient through } y_i^j$ */

$L(\theta) \leftarrow \frac{1}{B} \sum_{i=1}^B \min\{\frac{\pi_{\theta}(A_i|S_i)}{\pi_{\theta_{old}}(A_i|S_i)} \text{Adv}_i, \text{clip}(\frac{\pi_{\theta}(A_i|S_i)}{\pi_{\theta_{old}}(A_i|S_i)}) \text{Adv}_i\}$;

Perform one gradient update to ψ minimizing $L(\psi)$ with Adam;

if $\frac{1}{B} \sum_{i=1}^B \log \pi_{\theta_{old}}(A_i|S_i) - \log \pi_{\theta}(A_i|S_i) < KL_{target}$ **then**

 Perform one gradient update to θ maximizing $L(\theta)$ with Adam;

end

end**end**

Algorithm 5: DisPPO

Input: θ, ψ : parameters of π, \hat{v} ; α_A, α_C : Initial learning rates of the Adam optimizers for θ, ψ ; K, K_{opt}, B : rollout length, number of optimization epochs, and minibatch size; KL_{target} : maximum KL divergence threshold

;

 $S_0 \sim \mu_0, t \leftarrow 0$ **while** *True* **do** Initialize a buffer M ; $\theta_{old} \leftarrow \theta$; **for** $i = 0, \dots, K - 1$ **do** $A_i \sim \pi_{\theta_{old}}(\cdot|S_i), t_i \leftarrow t$; Execute A_i , get R_{i+1}, S_{i+1} ; **if** S_{i+1} is a terminal state **then** $m_i \leftarrow 0, S_{i+1} \sim \mu_0, t \leftarrow 0$ **else** $m_i \leftarrow 1, t \leftarrow t + 1$ **end** **end** $G_K \leftarrow \hat{v}(S_K)$; **for** $i = K - 1, \dots, 0$ **do** $G_i \leftarrow R_{i+1} + \gamma_C m_i G_{i+1}$; $\text{Adv}_i \leftarrow R_{i+1} + \gamma_C m_i \hat{v}_\psi(S_{i+1}) - \hat{v}_\psi(S_i)$; Store $(S_i, A_i, G_i, \text{Adv}_i, t_i)$ in M ; **end** Normalize Adv_i in M as $\text{Adv}_i \leftarrow \frac{\text{Adv}_i - \text{mean}(\{\text{Adv}_i\})}{\text{std}(\{\text{Adv}_i\})}$; **for** $o = 1, \dots, K_{opt}$ **do** Sample a minibatch $\{(S_i, A_i, G_i, \text{Adv}_i, t_i)\}_{i=1, \dots, B}$ from M ; $L(\psi) \leftarrow \frac{1}{2B} \sum_{i=1}^B (\hat{v}_\psi(S_i) - G_i)^2$ /* No gradient through G_i */ $L(\theta) \leftarrow \frac{1}{B} \sum_{i=1}^B \gamma_A^{t_i} \min\{\frac{\pi_\theta(A_i|S_i)}{\pi_{\theta_{old}}(A_i|S_i)} \text{Adv}_i, \text{clip}(\frac{\pi_\theta(A_i|S_i)}{\pi_{\theta_{old}}(A_i|S_i)}) \text{Adv}_i\}$; Perform one gradient update to ψ minimizing $L(\psi)$ with Adam; **if** $\frac{1}{B} \sum_{i=1}^B \log \pi_{\theta_{old}}(A_i|S_i) - \log \pi_\theta(A_i|S_i) < KL_{target}$ **then** Perform one gradient update to θ maximizing $L(\theta)$ with Adam; **end** **end****end**

Algorithm 6: AuxPPO

Input: θ, θ', ψ : parameters of π, π', \hat{v} ; α_A, α_C : Initial learning rates of the Adam optimizers for θ, ψ ; K, K_{opt}, B : rollout length, number of optimization epochs, and minibatch size; KL_{target} : maximum KL divergence threshold

;

 $S_0 \sim \mu_0, t \leftarrow 0$ **while** *True* **do**Initialize a buffer M ; $\theta_{old} \leftarrow \theta, \theta' \leftarrow \theta$;**for** $i = 0, \dots, K - 1$ **do** $A_i \sim \pi_{\theta_{old}}(\cdot|S_i), t_i \leftarrow t$;Execute A_i , get R_{i+1}, S_{i+1} ;**if** S_{i+1} is a terminal state **then**| $m_i \leftarrow 0, S_{i+1} \sim \mu_0, t \leftarrow 0$ **else**| $m_i \leftarrow 1, t \leftarrow t + 1$ **end****end** $G_K \leftarrow \hat{v}(S_K)$;**for** $i = K - 1, \dots, 0$ **do** $G_i \leftarrow R_{i+1} + \gamma_C m_i G_{i+1}$; $\text{Adv}_i \leftarrow R_{i+1} + \gamma_C m_i \hat{v}_\psi(S_{i+1}) - \hat{v}_\psi(S_i)$;Store $(S_i, A_i, G_i, \text{Adv}_i, t_i)$ in M ;**end**Normalize Adv_i in M as $\text{Adv}_i \leftarrow \frac{\text{Adv}_i - \text{mean}(\{\text{Adv}_i\})}{\text{std}(\{\text{Adv}_i\})}$;**for** $o = 1, \dots, K_{opt}$ **do**Sample a minibatch $\{(S_i, A_i, G_i, \text{Adv}_i, t_i)\}_{i=1, \dots, B}$ from M ; $L(\psi) \leftarrow \frac{1}{2B} \sum_{i=1}^B (\hat{v}_\psi(S_i) - G_i)^2$ /* No gradient through G_i */

*/

$$L(\theta, \theta') \leftarrow \frac{1}{B} \sum_{i=1}^B \gamma_C^{t_i} \min\left\{ \frac{\pi_\theta(A_i|S_i)}{\pi_{\theta_{old}}(A_i|S_i)} \text{Adv}_i, \text{clip}\left(\frac{\pi_\theta(A_i|S_i)}{\pi_{\theta_{old}}(A_i|S_i)}\right) \text{Adv}_i \right\} + \\ (1 - \gamma_C^{t_i}) \min\left\{ \frac{\pi_{\theta'}(A_i|S_i)}{\pi_{\theta_{old}}(A_i|S_i)} \text{Adv}_i, \text{clip}\left(\frac{\pi_{\theta'}(A_i|S_i)}{\pi_{\theta_{old}}(A_i|S_i)}\right) \text{Adv}_i \right\}$$

;

Perform one gradient update to ψ minimizing $L(\psi)$ with Adam;**if** $\frac{1}{B} \sum_{i=1}^B \log \pi_{\theta_{old}}(A_i|S_i) - \log \pi_\theta(A_i|S_i) < KL_{target}$ **then**| Perform one gradient update to θ, θ' maximizing $L(\theta, \theta')$ with Adam;**end****end****end**

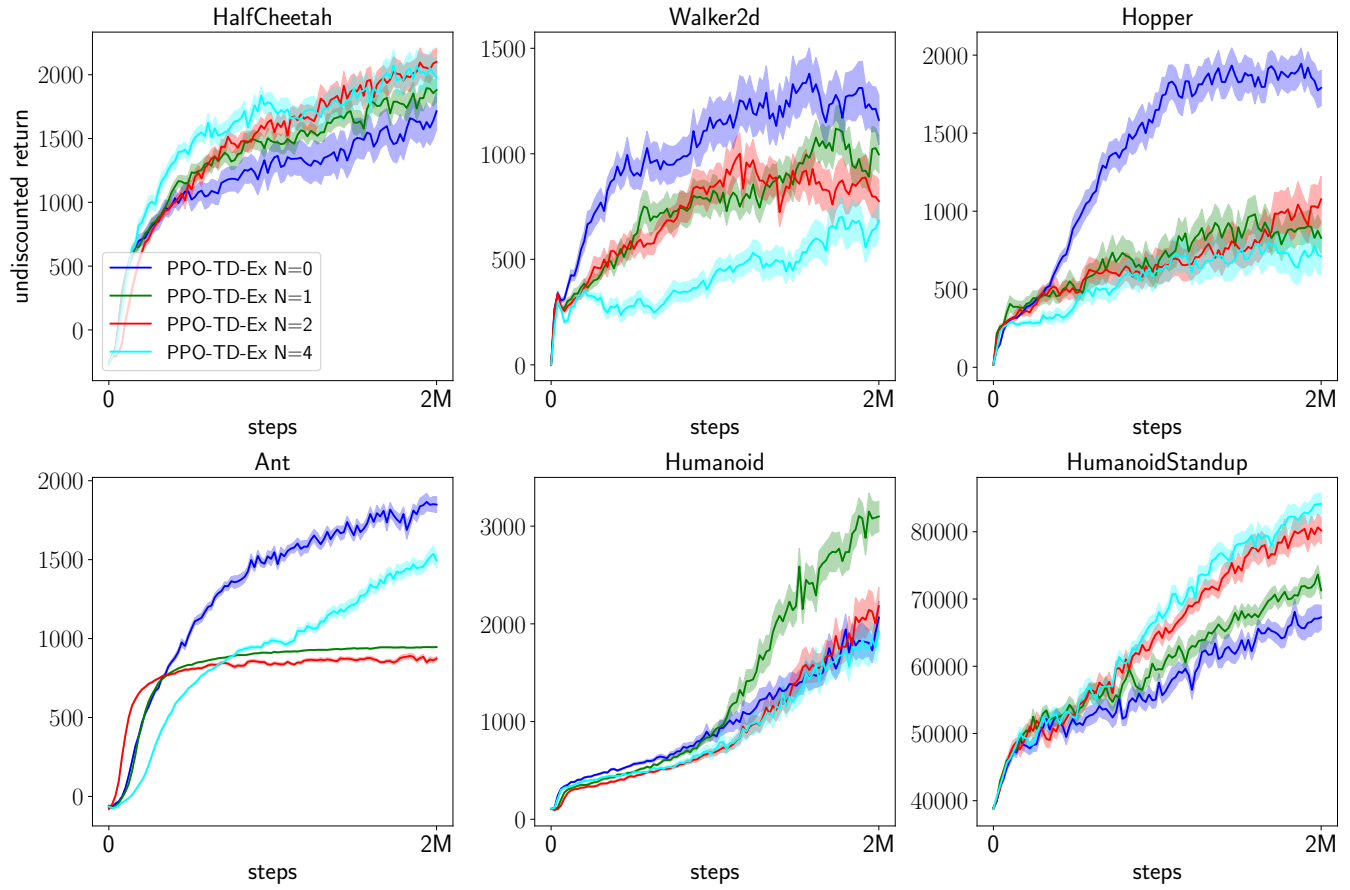


Figure 13: PPO-TD-Ex ($\gamma_c = 0.995$).

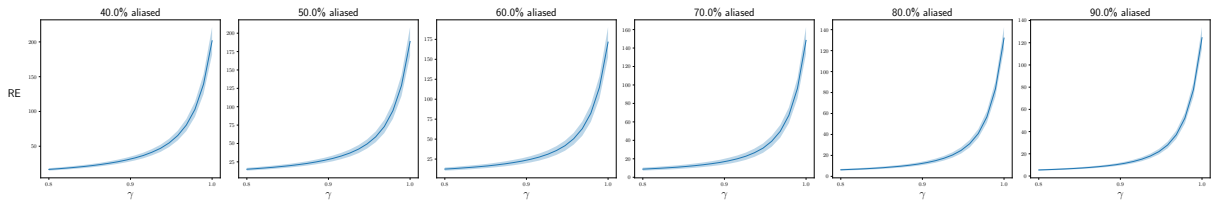


Figure 14: Unnormalized representation error (RE) as a function of the discount factor. Shaded regions indicate one standard derivation. RE is computed analytically as

$$\text{RE}(X, \gamma) \doteq \min_w \|Xw - v_\gamma\|_2$$

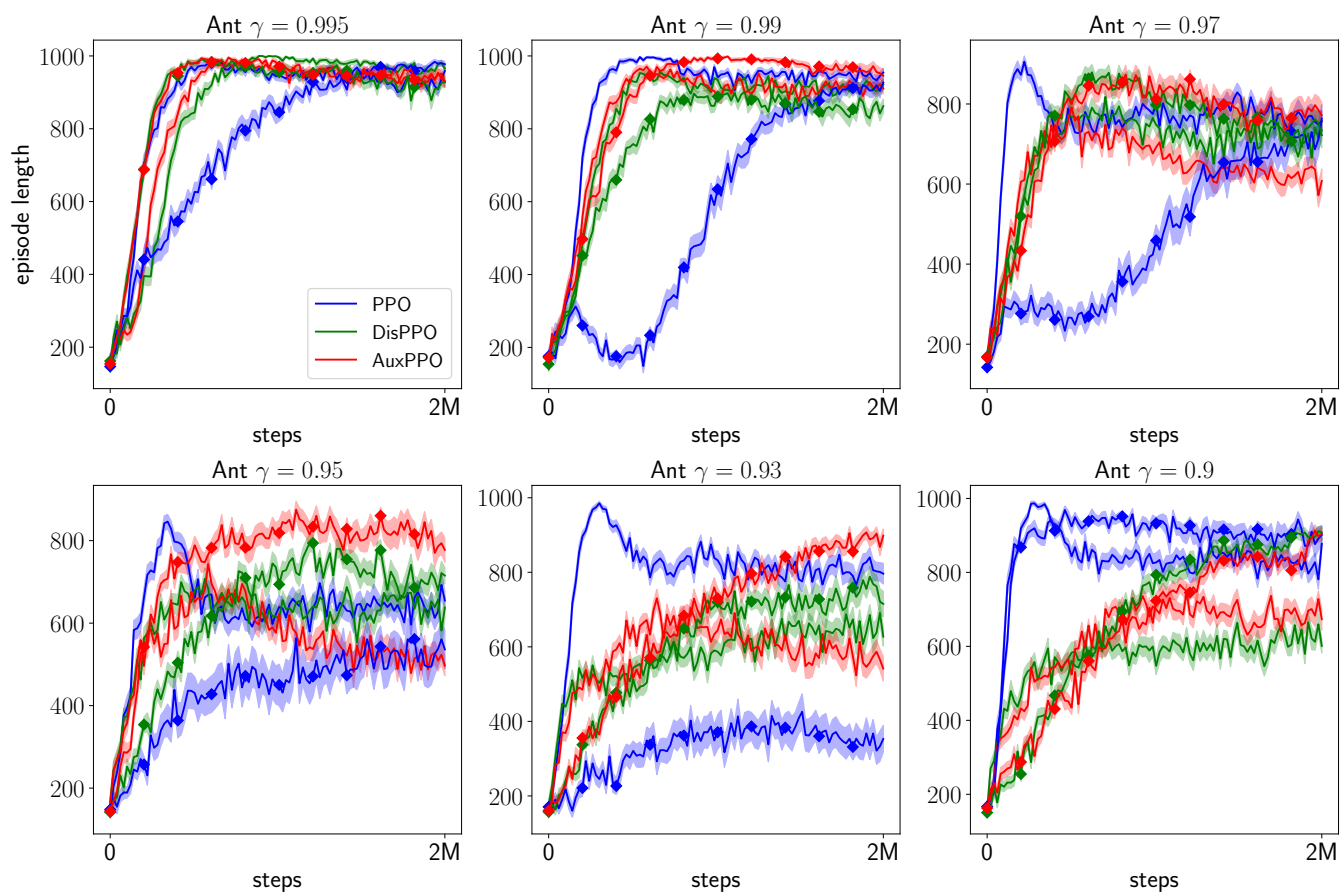


Figure 15: Curves without any marker are obtained in the original Ant. Diamond-marked curves are obtained in Ant with r' .

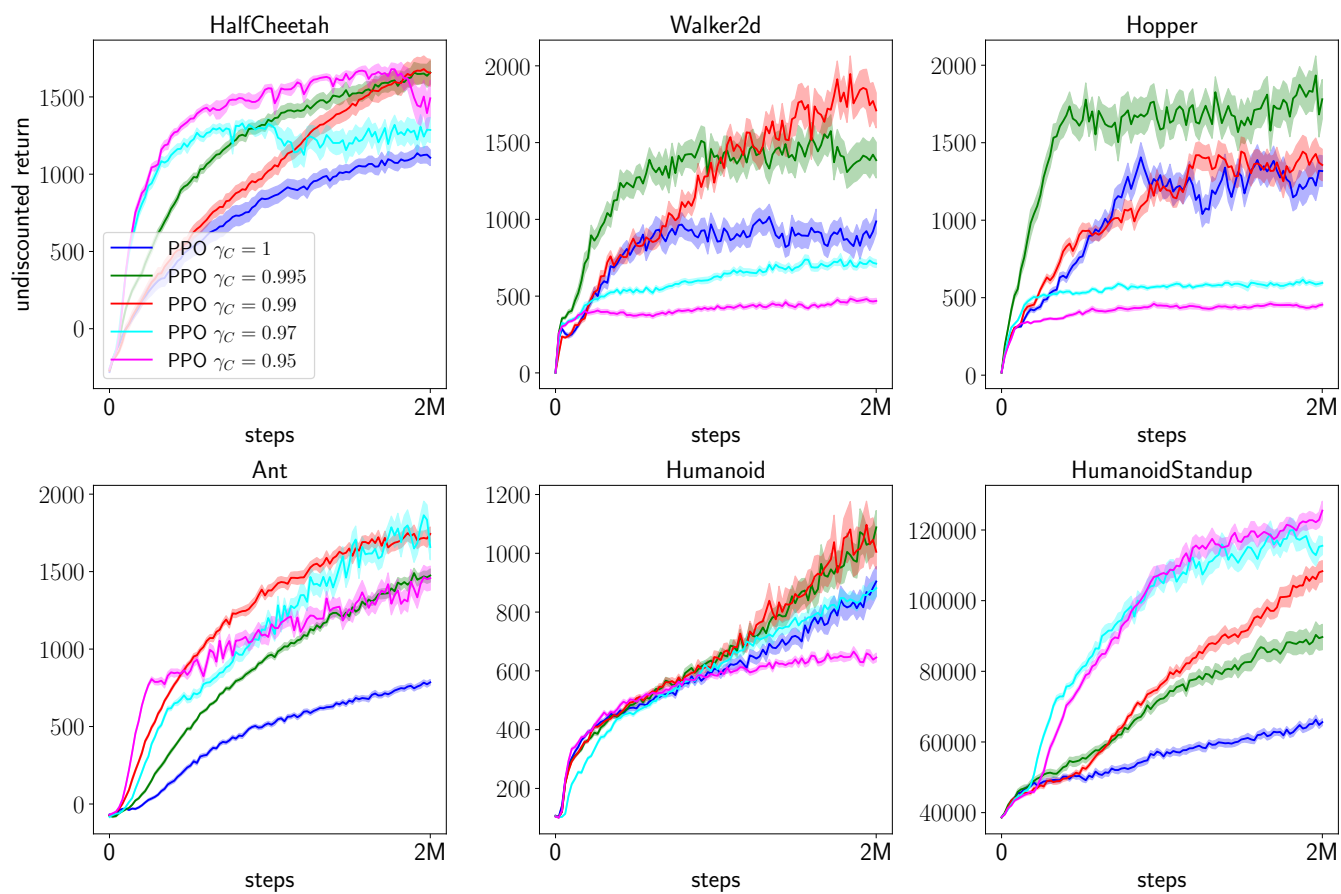


Figure 16: The default PPO implementation with different discount factors. The larger version of Figure 1.

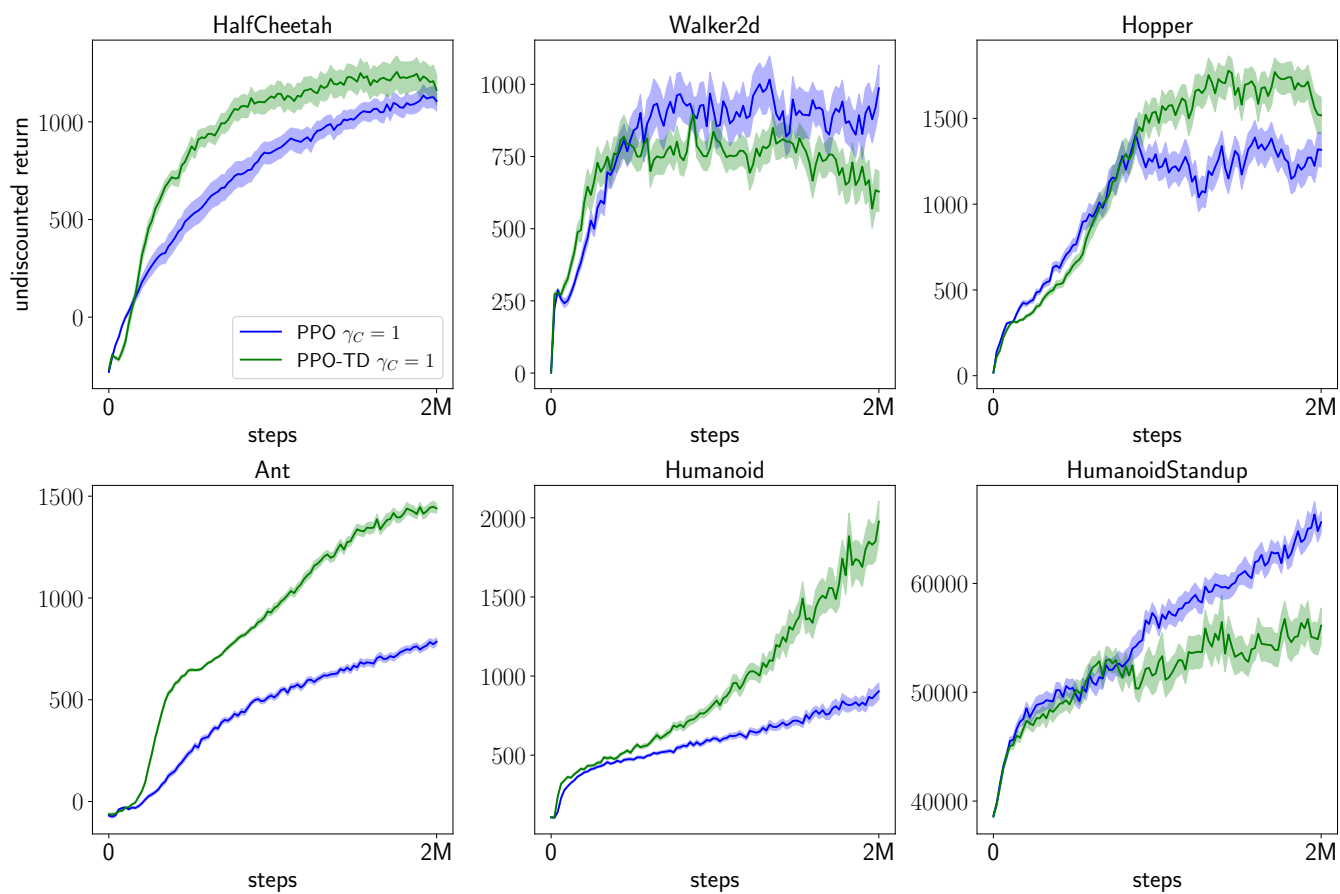


Figure 17: Comparison between PPO and PPO-TD when $\gamma_c = 1$. The larger version of Figure 2.

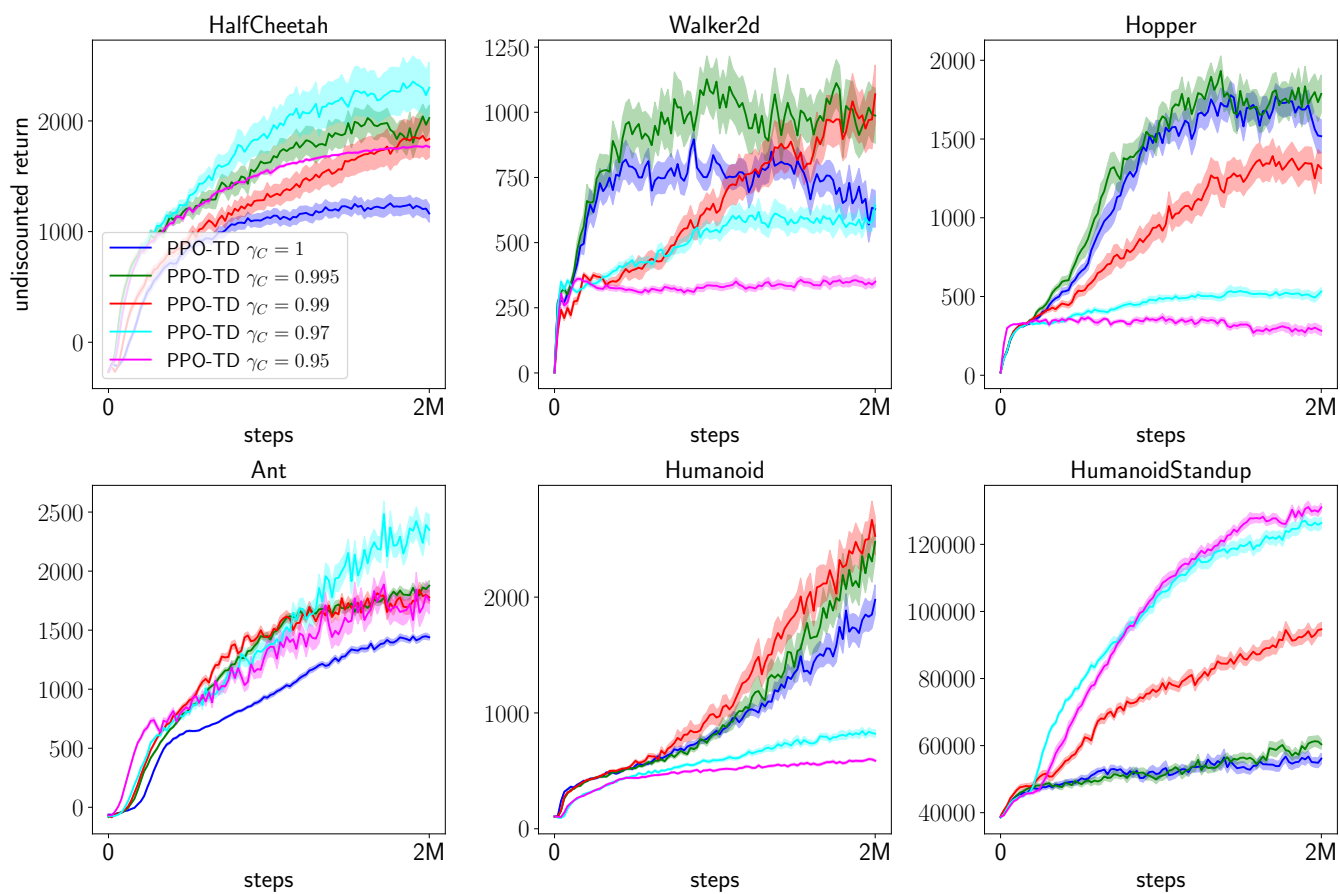


Figure 18: PPO-TD with different discount factors. The larger version of Figure 3.

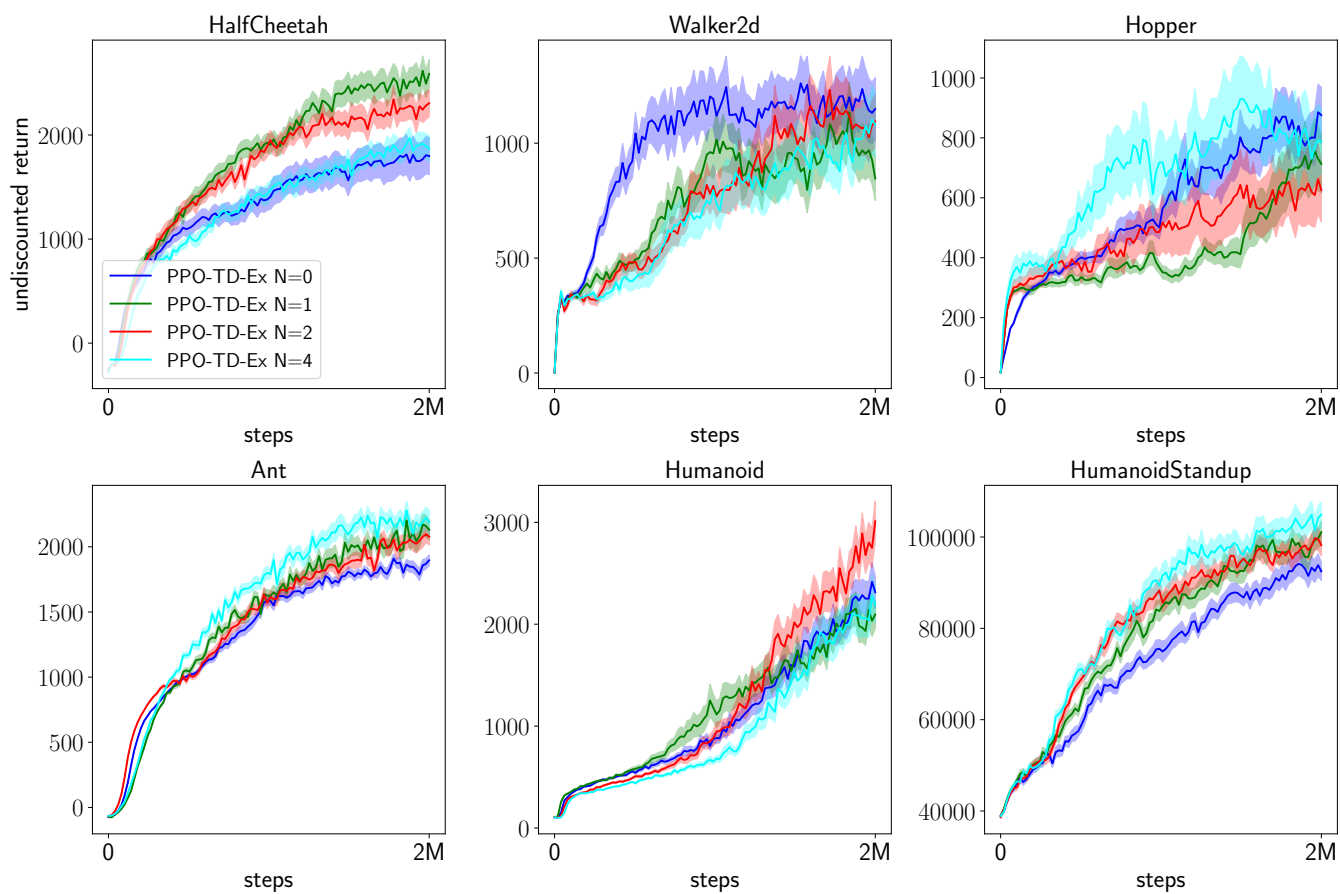


Figure 19: PPO-TD-Ex ($\gamma_c = 0.99$). The larger version of Figure 4.

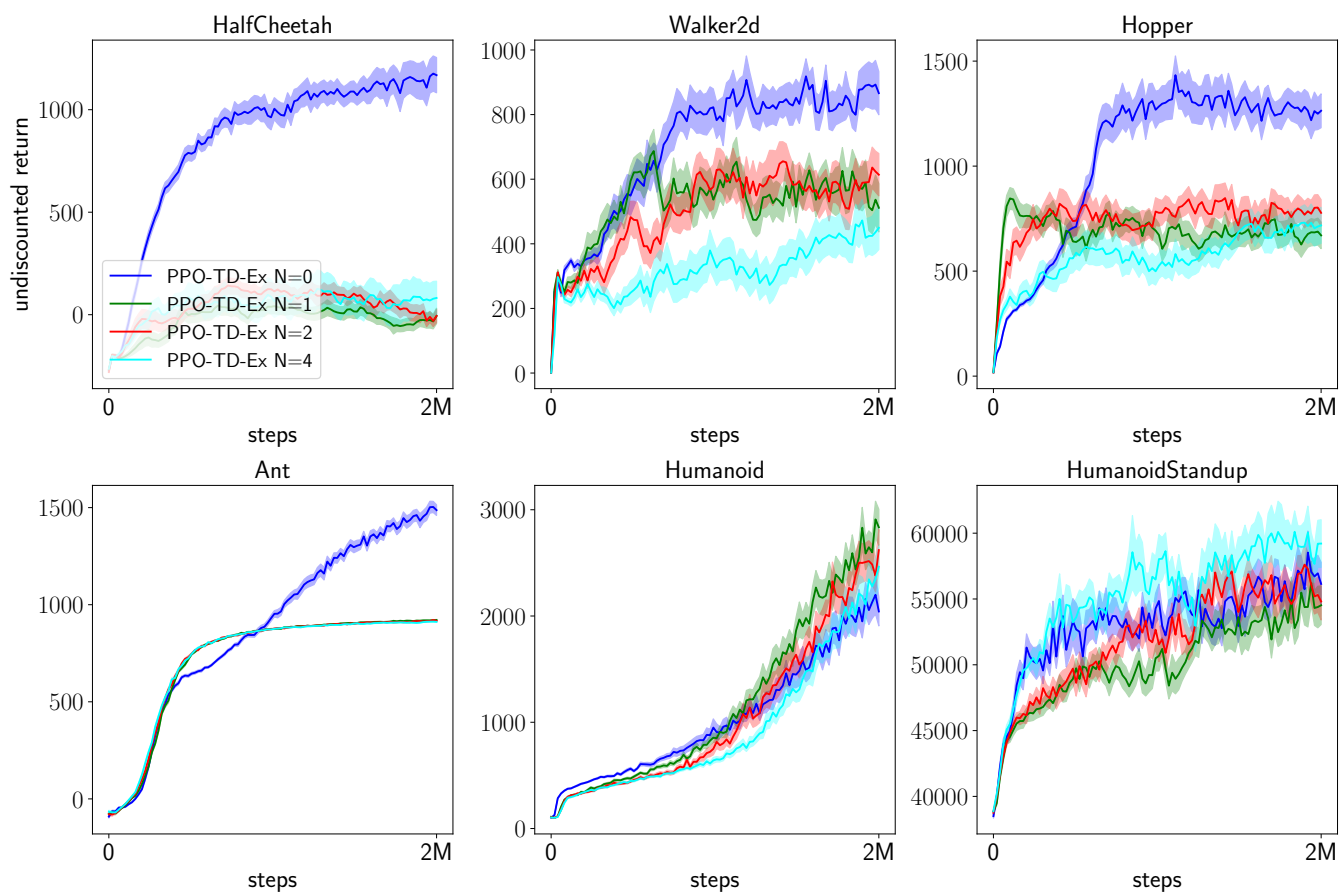


Figure 20: PPO-TD-Ex ($\gamma_c = 1$). The larger version of Figure 5.

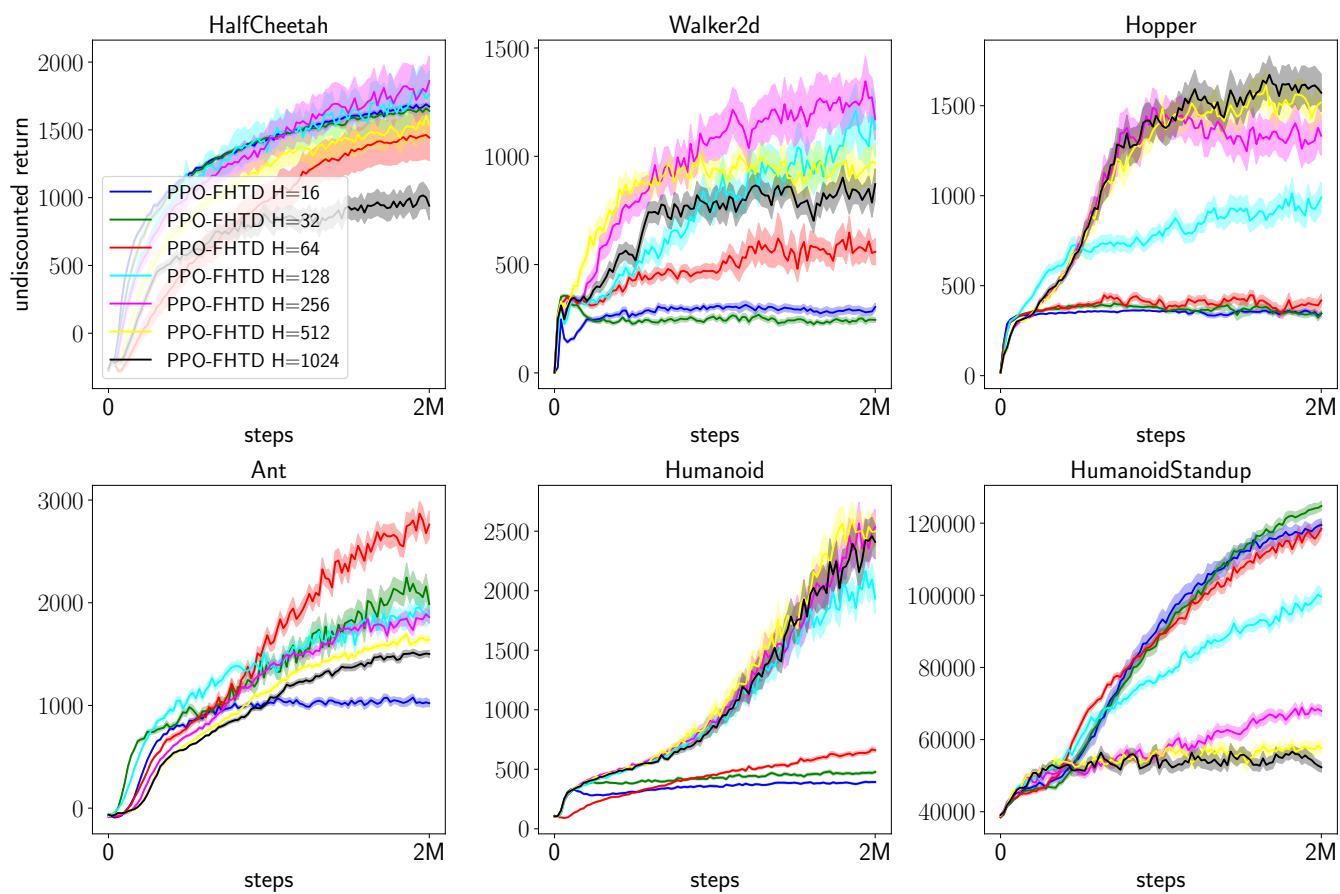


Figure 21: PPO-FHTD with the first parameterization. The best H and γ_c are used for each game. The larger version of Figure 6.

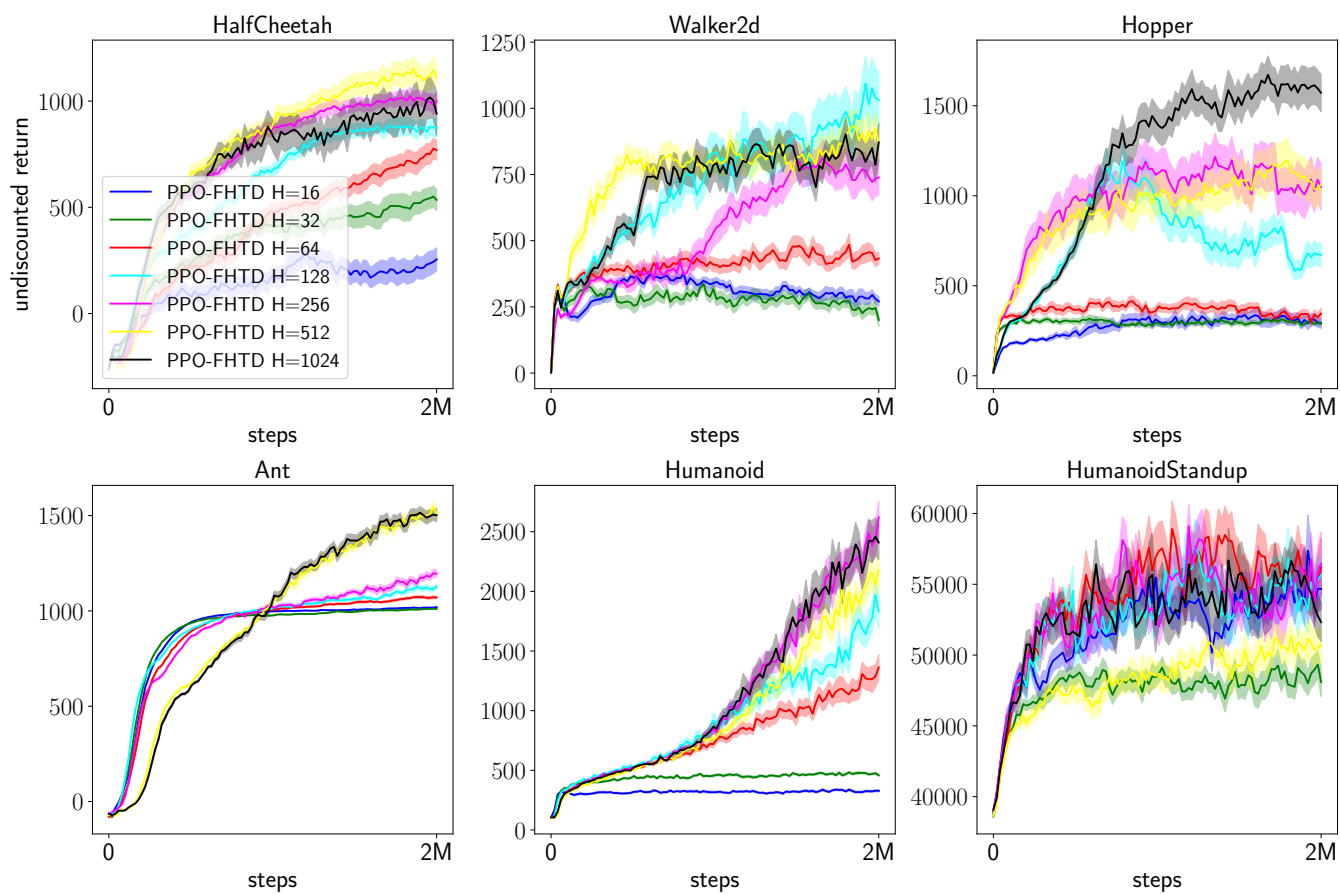


Figure 22: PPO-FHTD with the second parameterization. The larger version of Figure 7.

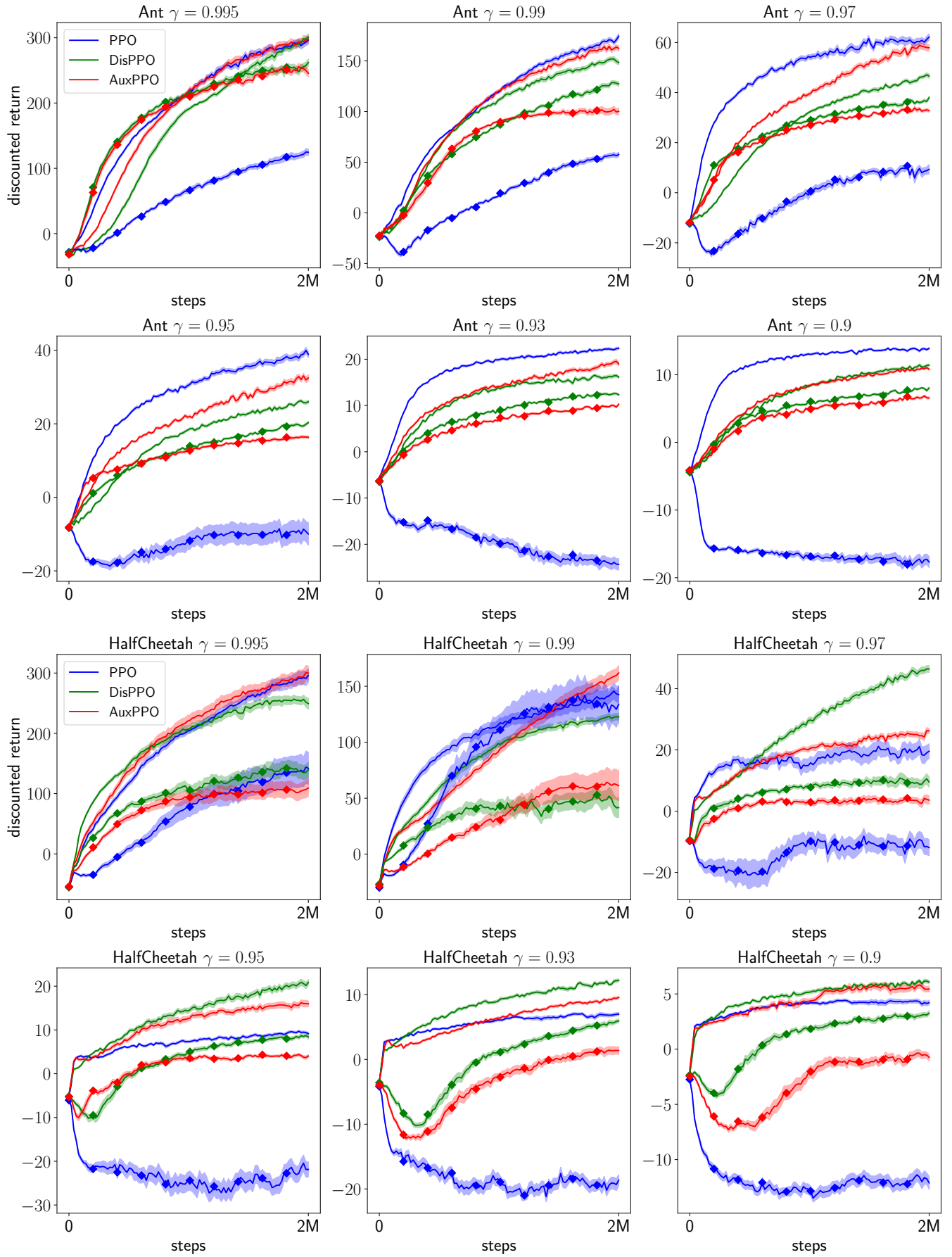


Figure 23: Curves without any marker are obtained in the original Ant environment. Diamond-marked curves are obtained in Ant with r' . The larger version of Figure 11.